EUROPEAN ORGANISATION FOR NUCLEAR RESEARCH

CERN-PPE/96-47
26 March 1996

QCD studies with e^+e^- annihilation data at 130 and 136 GeV

The OPAL Collaboration

Abstract

We have studied hadronic events produced at LEP at centre-of-mass energies of 130 and 136 GeV. Distributions of event shape observables, jet rates, momentum spectra and multiplicities are presented and compared to the predictions of several Monte Carlo models and analytic QCD calculations. From fits of event shape and jet rate distributions to $\mathcal{O}(\alpha_s^2)$+NLLA QCD calculations, we determine $\alpha_s(133\ \mathrm{GeV}) = 0.110 \pm 0.005(\mathrm{stat.}) \pm 0.009(\mathrm{syst.})$. We measure the mean charged particle multiplicity $\langle n_{\mathrm{ch}} \rangle = 23.40 \pm 0.45(\mathrm{stat.}) \pm 0.47(\mathrm{syst.})$ and the position ξ_0 of the peak in the $\xi_p = \ln(1/x_p)$ distribution $\xi_0 = 3.94 \pm 0.05(\mathrm{stat.}) \pm 0.11(\mathrm{syst.})$. These results are compared to lower energy data and to analytic QCD or Monte Carlo predictions for their energy evolution.

Submitted to Zeitschrift für Physik C

The OPAL Collaboration

G. Alexander[23], J. Allison[16], N. Altekamp[5], K. Ametewee[25], K.J. Anderson[9], S. Anderson[12], S. Arcelli[2], S. Asai[24], D. Axen[29], G. Azuelos[18,a], A.H. Ball[17], E. Barberio[26], R.J. Barlow[16], R. Bartoldus[3], J.R. Batley[5], G. Beaudoin[18], J. Bechtluft[14], C. Beeston[16], T. Behnke[8], A.N. Bell[1], K.W. Bell[20], G. Bella[23], S. Bentvelsen[8], P. Berlich[10], S. Bethke[14], O. Biebel[14], V. Blobel[8], I.J. Bloodworth[1], J.E. Bloomer[1], P. Bock[11], H.M. Bosch[11], M. Boutemeur[18], B.T. Bouwens[12], S. Braibant[12], R.M. Brown[20], H.J. Burckhart[8], C. Burgard[27], R. Bürgin[10], P. Capiluppi[2], R.K. Carnegie[6], A.A. Carter[13], J.R. Carter[5], C.Y. Chang[17], C. Charlesworth[6], D.G. Charlton[1,b], D. Chrisman[4], S.L. Chu[4], P.E.L. Clarke[15], I. Cohen[23], J.E. Conboy[15], O.C. Cooke[16], M. Cuffiani[2], S. Dado[22], C. Dallapiccola[17], G.M. Dallavalle[2], S. De Jong[12], L.A. del Pozo[8], K. Desch[3], M.S. Dixit[7], E. do Couto e Silva[12], M. Doucet[18], E. Duchovni[26], G. Duckeck[8], I.P. Duerdoth[16], J.E.G. Edwards[16], P.G. Estabrooks[6], H.G. Evans[9], M. Evans[13], F. Fabbri[2], P. Fath[11], F. Fiedler[12], M. Fierro[2], H.M. Fischer[3], R. Folman[26], D.G. Fong[17], M. Foucher[17], H. Fukui[24], A. Fürtjes[8], P. Gagnon[7], A. Gaidot[21], J.W. Gary[4], J. Gascon[18], S.M. Gascon-Shotkin[17], N.I. Geddes[20], C. Geich-Gimbel[3], F.X. Gentit[21], T. Geralis[20], G. Giacomelli[2], P. Giacomelli[4], R. Giacomelli[2], V. Gibson[5], W.R. Gibson[13], D.M. Gingrich[30,a], J. Goldberg[22], M.J. Goodrick[5], W. Gorn[4], C. Grandi[2], E. Gross[26], M. Gruwé[8], C. Hajdu[32], G.G. Hanson[12], M. Hansroul[8], M. Hapke[13], C.K. Hargrove[7], P.A. Hart[9], C. Hartmann[3], M. Hauschild[8], C.M. Hawkes[5], R. Hawkings[8], R.J. Hemingway[6], G. Herten[10], R.D. Heuer[8], M.D. Hildreth[8], J.C. Hill[5], S.J. Hillier[1], T. Hilse[10], J. Hoare[5], P.R. Hobson[25], R.J. Homer[1], A.K. Honma[28,a], D. Horváth[32,c], R. Howard[29], R.E. Hughes-Jones[16], D.E. Hutchcroft[5], P. Igo-Kemenes[11], D.C. Imrie[25], M.R. Ingram[16], A. Jawahery[17], P.W. Jeffreys[20], H. Jeremie[18], M. Jimack[1], A. Joly[18], C.R. Jones[5], G. Jones[16], M. Jones[6], R.W.L. Jones[8], U. Jost[11], P. Jovanovic[1], T.R. Junk[8], D. Karlen[6], K. Kawagoe[24], T. Kawamoto[24], R.K. Keeler[28], R.G. Kellogg[17], B.W. Kennedy[20], B.J. King[8], J. Kirk[29], S. Kluth[8], T. Kobayashi[24], M. Kobel[10], D.S. Koetke[6], T.P. Kokott[3], S. Komamiya[24], R. Kowalewski[8], T. Kress[11], P. Krieger[6], J. von Krogh[11], P. Kyberd[13], G.D. Lafferty[16], H. Lafoux[21], R. Lahmann[17], W.P. Lai[19], D. Lanske[14], J. Lauber[15], S.R. Lautenschlager[31], J.G. Layter[4], D. Lazic[22], A.M. Lee[31], E. Lefebvre[18], D. Lellouch[26], J. Letts[2], L. Levinson[26], C. Lewis[15], S.L. Lloyd[13], F.K. Loebinger[16], G.D. Long[17], M.J. Losty[7], J. Ludwig[10], A. Luig[10], A. Malik[21], M. Mannelli[8], S. Marcellini[2], C. Markus[3], A.J. Martin[13], J.P. Martin[18], G. Martinez[17], T. Mashimo[24], W. Matthews[25], P. Mättig[3], W.J. McDonald[30], J. McKenna[29], E.A. Mckigney[15], T.J. McMahon[1], A.I. McNab[13], R.A. McPherson[8], F. Meijers[8], S. Menke[3], F.S. Merritt[9], H. Mes[7], J. Meyer[27], A. Michelini[2], G. Mikenberg[26], D.J. Miller[15], R. Mir[26], W. Mohr[10], A. Montanari[2], T. Mori[24], M. Morii[24], U. Müller[3], H.A. Neal[8], B. Nellen[3], B. Nijjhar[16], R. Nisius[8], S.W. O'Neale[1], F.G. Oakham[7], F. Odorici[2], H.O. Ogren[12], T. Omori[24], M.J. Oreglia[9], S. Orito[24], J. Pálinkás[33,d], J.P. Pansart[21], G. Pásztor[32], J.R. Pater[16], G.N. Patrick[20], M.J. Pearce[1], S. Petzold[27], P. Pfeifenschneider[14], J.E. Pilcher[9], J. Pinfold[30], D.E. Plane[8], P. Poffenberger[28], B. Poli[2],

A. Posthaus[3], H. Przysiezniak[30], D.L. Rees[1], D. Rigby[1], S.A. Robins[13], N. Rodning[30], J.M. Roney[28], A. Rooke[15], E. Ros[8], A.M. Rossi[2], M. Rosvick[28], P. Routenburg[30], Y. Rozen[8], K. Runge[10], O. Runolfsson[8], U. Ruppel[14], D.R. Rust[12], R. Rylko[25], E.K.G. Sarkisyan[23], M. Sasaki[24], C. Sbarra[2], A.D. Schaile[8,e], O. Schaile[10], F. Scharf[3], P. Scharff-Hansen[8], P. Schenk[4], B. Schmitt[3], S. Schmitt[11], M. Schröder[8], H.C. Schultz-Coulon[10], M. Schulz[8], P. Schütz[3], W.G. Scott[20], T.G. Shears[16], B.C. Shen[4], C.H. Shepherd-Themistocleous[27], P. Sherwood[15], G.P. Siroli[2], A. Sittler[27], A. Skillman[15], A. Skuja[17], A.M. Smith[8], T.J. Smith[28], G.A. Snow[17], R. Sobie[28], S. Söldner-Rembold[10], R.W. Springer[30], M. Sproston[20], A. Stahl[3], M. Starks[12], M. Steiert[11], K. Stephens[16], J. Steuerer[27], B. Stockhausen[3], D. Strom[19], F. Strumia[8], P. Szymanski[20], R. Tafirout[18], S.D. Talbot[1], S. Tanaka[24], P. Taras[18], S. Tarem[22], M. Tecchio[8], M. Thiergen[10], M.A. Thomson[8], E. von Törne[3], S. Towers[6], M. Tscheulin[10], T. Tsukamoto[24], E. Tsur[23], A.S. Turcot[9], M.F. Turner-Watson[8], P. Utzat[11], R. Van Kooten[12], G. Vasseur[21], M. Verzocchi[10], P. Vikas[18], M. Vincter[28], E.H. Vokurka[16], F. Wäckerle[10], A. Wagner[27], C.P. Ward[5], D.R. Ward[5], J.J. Ward[15], P.M. Watkins[1], A.T. Watson[1], N.K. Watson[7], P. Weber[6], P.S. Wells[8], N. Wermes[3], J.S. White[28], B. Wilkens[10], G.W. Wilson[27], J.A. Wilson[1], T. Wlodek[26], G. Wolf[26], S. Wotton[5], T.R. Wyatt[16], S. Yamashita[24], G. Yekutieli[26], V. Zacek[18],

[1]School of Physics and Space Research, University of Birmingham, Birmingham B15 2TT, UK
[2]Dipartimento di Fisica dell' Università di Bologna and INFN, I-40126 Bologna, Italy
[3]Physikalisches Institut, Universität Bonn, D-53115 Bonn, Germany
[4]Department of Physics, University of California, Riverside CA 92521, USA
[5]Cavendish Laboratory, Cambridge CB3 0HE, UK
[6] Ottawa-Carleton Institute for Physics, Department of Physics, Carleton University, Ottawa, Ontario K1S 5B6, Canada
[7]Centre for Research in Particle Physics, Carleton University, Ottawa, Ontario K1S 5B6, Canada
[8]CERN, European Organisation for Particle Physics, CH-1211 Geneva 23, Switzerland
[9]Enrico Fermi Institute and Department of Physics, University of Chicago, Chicago IL 60637, USA
[10]Fakultät für Physik, Albert Ludwigs Universität, D-79104 Freiburg, Germany
[11]Physikalisches Institut, Universität Heidelberg, D-69120 Heidelberg, Germany
[12]Indiana University, Department of Physics, Swain Hall West 117, Bloomington IN 47405, USA
[13]Queen Mary and Westfield College, University of London, London E1 4NS, UK
[14]Technische Hochschule Aachen, III Physikalisches Institut, Sommerfeldstrasse 26-28, D-52056 Aachen, Germany
[15]University College London, London WC1E 6BT, UK
[16]Department of Physics, Schuster Laboratory, The University, Manchester M13 9PL, UK
[17]Department of Physics, University of Maryland, College Park, MD 20742, USA

[18]Laboratoire de Physique Nucléaire, Université de Montréal, Montréal, Quebec H3C 3J7, Canada
[19]University of Oregon, Department of Physics, Eugene OR 97403, USA
[20]Rutherford Appleton Laboratory, Chilton, Didcot, Oxfordshire OX11 0QX, UK
[21]CEA, DAPNIA/SPP, CE-Saclay, F-91191 Gif-sur-Yvette, France
[22]Department of Physics, Technion-Israel Institute of Technology, Haifa 32000, Israel
[23]Department of Physics and Astronomy, Tel Aviv University, Tel Aviv 69978, Israel
[24]International Centre for Elementary Particle Physics and Department of Physics, University of Tokyo, Tokyo 113, and Kobe University, Kobe 657, Japan
[25]Brunel University, Uxbridge, Middlesex UB8 3PH, UK
[26]Particle Physics Department, Weizmann Institute of Science, Rehovot 76100, Israel
[27]Universität Hamburg/DESY, II Institut für Experimental Physik, Notkestrasse 85, D-22607 Hamburg, Germany
[28]University of Victoria, Department of Physics, P O Box 3055, Victoria BC V8W 3P6, Canada
[29]University of British Columbia, Department of Physics, Vancouver BC V6T 1Z1, Canada
[30]University of Alberta, Department of Physics, Edmonton AB T6G 2J1, Canada
[31]Duke University, Dept of Physics, Durham, NC 27708-0305, USA
[32]Research Institute for Particle and Nuclear Physics, H-1525 Budapest, P O Box 49, Hungary
[33]Institute of Nuclear Research, H-4001 Debrecen, P O Box 51, Hungary

[a] and at TRIUMF, Vancouver, Canada V6T 2A3
[b] and Royal Society University Research Fellow
[c] and Institute of Nuclear Research, Debrecen, Hungary
[d] and Department of Experimental Physics, Lajos Kossuth University, Debrecen, Hungary
[e] and Ludwig-Maximilians-Universität, München, Germany

1 Introduction

In 1995 the LEP e^+e^- collider was upgraded from a centre-of-mass energy of $\sqrt{s} \simeq 91$ GeV to $\sqrt{s} = 130-140$ GeV. This allowed the study of hadronic events produced in the process $e^+e^- \to (Z^0/\gamma^*) \to$ hadrons at larger energies than had previously been possible in e^+e^- collisions. Two main effects are expected to influence QCD observables at the higher centre-of-mass energies: the running of the strong coupling α_s, i.e. its dependence on the energy scale of the process, and the change of quark flavour composition compared to events produced at the Z^0 peak. According to the Standard Model, α_s should decrease by about 5% between 91 and 130 GeV and the fraction of up-type quarks should change from about 34% at the Z^0 peak to 45% at 130 GeV (in events without initial state radiation). In addition, the effects of hadronisation are predicted to be smaller at higher centre-of-mass energies, and therefore perturbative QCD predictions might be expected to give a better description of experimental data.

Hadronic events can be characterised by event shape distributions and inclusive observables such as jet rates, momentum spectra and charged particle multiplicities. The comparison of these experimental data with the predictions of QCD Monte Carlo models and analytic calculations is a test of the overall consistency of QCD in this new energy regime. Deviations from the predictions might indicate deficiencies of a particular Monte Carlo model or the presence of unexpected physical processes. Some of these observables are described by analytic QCD predictions, from which a value for the strong coupling constant α_s at the higher energy scale may be determined. It is an important test of QCD that each of these observables can be described by the same value of α_s, and that this is consistent with measurements of α_s from lower energy data when evolved to $\sqrt{s} = M_{Z^0}$. Other observables, such as the charged particle multiplicity and the momentum spectrum of soft particles, are described by analytic calculations based on the Leading Logarithmic Approximation (LLA). These calculations predict the energy evolution of the data and therefore can be tested by comparing the current measurements with lower energy data.

A large fraction of the hadronic data collected at energies above the Z^0 are events in which the radiation of a hard photon from the e^+e^- initial state (initial state radiation) results in the resonant production of a Z^0 boson. These events, with an effective centre-of-mass energy of $\sqrt{s'} \sim 91$ GeV, are expected to correspond to the same physical processes as the LEP I data. In order to study the energy evolution of QCD observables, the energy at which the hadronic system is produced should be monochromatic to within a few GeV, and therefore a separation between "radiative" and "non-radiative" events is essential.

In the following sections we describe briefly the OPAL detector and the event samples on which our studies are based. We describe the cuts used to select the data and the correction procedures applied to them, and discuss the event shape and jet rate distributions. A subset of the event shape and jet rate distributions is then compared with QCD predictions to extract a value of α_s. Distributions based on measurements of charged tracks are then presented. Finally, we compare our findings for the mean charged particle multiplicity, the position of the peak in the $\ln(1/x_p)$ distribution, the 3-jet rate, the mean value of thrust and the value of α_s with lower energy data and QCD predictions.

2 The OPAL detector

The OPAL detector operates at the LEP e^+e^- collider at CERN. A detailed description can be found in reference [1]. The analysis presented here relies mainly on the measurements of momenta and directions of charged tracks in the tracking chambers and of energy deposited in the electromagnetic and hadronic calorimeters of the detector.

All tracking systems are located inside a solenoidal magnet which provides a uniform axial magnetic field of 0.435 T along the beam axis[1]. The magnet is surrounded by a lead glass electromagnetic calorimeter and a hadron calorimeter of the sampling type. Outside the hadron calorimeter, the detector is surrounded by a system of muon chambers. There are similar layers of detectors in the forward and backward endcaps.

The main tracking detector is the central jet chamber. This device is approximately 4 m long and has an outer radius of about 1.85 m. It has 24 sectors with radial planes of 159 sense wires spaced by 1 cm. The momenta, p, of tracks in the x-y plane are measured with a precision parametrised by $\sigma_p/p = \sqrt{0.02^2 + (0.0015 \cdot p[\mathrm{GeV}/c])^2}$.

The electromagnetic calorimeters in the barrel and the endcap sections of the detector consist of 11704 lead glass blocks with a depth of 24.6 radiation lengths in the barrel and more than 22 in the endcaps.

3 Data preselection and Monte Carlo samples

The data analysed in this paper were recorded in October and November 1995. We require the central jet chamber and the electromagnetic calorimeter to be fully operational. The identification of hadronic events is based on the criteria described in reference [2]. After this preselection, the data correspond to about 2.6 pb^{-1}, or 851 events, at $\sqrt{s}$=130.3 GeV and about 2.5 pb^{-1}, or 681 events, at $\sqrt{s}$=136.2 GeV.

Charged tracks and electromagnetic clusters are subjected to several quality cuts before further analysis. The tracks are required to have a transverse momentum with respect to the z axis greater than 0.15 GeV/c, a total momentum less than 90 GeV/c and at least 40 hits in the central jet chamber. In addition, the distance from the interaction region at the point of closest approach in r-ϕ must be less than 2 cm and the z coordinate at this point less than 25 cm. For clusters in the electromagnetic calorimeter, the energy is required to be at least 0.10 GeV in the barrel and 0.25 GeV in the endcap. The thrust axis (see section 5 below) is determined from all tracks and electromagnetic clusters passing these cuts. We apply a cut on the polar angle θ_T of the thrust axis to ensure that the events are well contained within the detector, by keeping only events with $|\cos\theta_T| < 0.9$.

Monte Carlo samples of hadronic events with full simulation of the OPAL detector [3] were generated at both energies. The generator used to simulate the events is PYTHIA 5.7 [4] with initial and final state photon radiation and with fragmentation of

[1] In the OPAL coordinate system the x axis points towards the centre of the LEP ring, the y axis points upwards and the z axis points in the direction of the electron beam. The polar angle θ and the azimuthal angle ϕ are defined w.r.t. z and y, respectively, while r is the distance from the z-axis.

the parton final state handled by the routines of JETSET 7.4 [4]. The samples contain 13 682 events at 130 GeV and 13 649 events at 136 GeV. The Monte Carlo parameters are tuned to OPAL data taken at the Z^0 peak [5].

Samples of Monte Carlo events generated with JETSET 7.4 with the same parameters and HERWIG 5.8 [6] with parameters given in reference [5] are used for studies of systematic uncertainties. JETSET and PYTHIA differ in the treatment of initial state radiation. For the HERWIG events we used the JETSET initial state radiation routines and hadron decay tables. Estimates of backgrounds from two-photon or tau pair events are derived from Monte Carlo simulations of these processes including full detector simulation. The Monte Carlo samples are analysed using the same reconstruction algorithms as are applied to the data.

4 Data analysis

In e^+e^- collisions, initial state radiation reduces the energy available to the $q\bar{q}$ system. Since the Z^0 resonance is below the nominal centre-of-mass energy, the cross-section is greatly enhanced for events in which the photon decreases the available energy such that an on-shell Z^0 boson is produced. The events therefore fall into two classes: those with a small amount of initial state radiation ("non-radiative events"), where the hadronic system has a centre-of-mass energy close to twice the beam energy; and "radiative events", where a large amount of radiation has allowed the production of a Z^0. Studies of QCD at the highest available energies require the events to be non-radiative, and therefore a procedure to select these events is necessary. This section describes the algorithms used to select events, the definition of the effective centre-of-mass energy and the corrections applied to the data.

4.1 Selection of non-radiative events

Initial state photons are expected to be produced predominantly along the beam direction. For a small fraction of events the photon may be identified in the detector, whereas for the majority of events the photon escapes undetected along the beam axis. In the latter case, we estimate the energy of the photon using a kinematic fit (c.f. [7]). The detected particles are first combined into jets using the Durham jet-finder [8] with a jet resolution of $y_{\rm cut} = 0.02$. If more than four jets are found, the required jet resolution is increased until the number of resolvable jets is four. The total energy of each jet is measured with information from the tracking chambers and the electromagnetic and hadron calorimeters, and is corrected with an algorithm which takes into account double counting of the energy of charged tracks [9]. Energy and momentum conservation are imposed in the fit, and the direction of initial state radiation is constrained to be approximately parallel to the beam axis. The fit determines the photon energy. For those events in which an isolated neutral cluster of at least 3 GeV is identified in the electromagnetic calorimeter, and which has a shape consistent with the expectation for a photon, the energy of the radiated photon is

taken to be the larger of the values observed in the calorimeter, or obtained from the fit.

The photon energy, E_γ, is used to compute the effective centre-of-mass energy, $\sqrt{s'}$, according to $s' = s - 2E_\gamma\sqrt{s}$. An event sample enhanced in non-radiative events is selected by requiring $\sqrt{s'} > \sqrt{s} - 10$ GeV.

From studies of simulated events using the PYTHIA event generator, we find that $\sqrt{s'}$ is determined with a resolution of about 3 GeV. The mean energy of initial state radiation in the selected events is 3.2 GeV at both 130 GeV and 136 GeV. If non-radiative events are defined as those generated with less than 5 GeV of radiation, the event selection is found to be 83% efficient with a background of 14% from radiative events.

An alternative selection is based on the observation that the radiative events have a reduced visible energy and a non-zero total momentum. Cuts are made on the visible energy $E_{\rm vis}$ and missing momentum $p_{\rm miss}$ in the event (again calculated according to the method described in reference [9]), scaled by the values which would be obtained for an event with radiative production of a real $\rm Z^0$ boson of mass $M_{\rm Z^0}$: $R_{\rm vis} = E_{\rm vis}/\sqrt{q_\gamma^2 + M_{\rm Z^0}^2}$ and $R_{\rm miss} = p_{\rm miss}/q_\gamma$, where $q_\gamma = (s - M_{\rm Z^0}^2)/2\sqrt{s}$. Non-radiative events are selected by requiring

$$\frac{R_{\rm vis} - R_{\rm miss}}{R_{\rm max}} > 0.5 \quad \text{and} \quad \frac{E_\gamma}{q_\gamma} < 0.4 \quad ,$$

where $R_{\rm max} = 2s/(s + M_{\rm Z^0}^2)$ is the maximal value of $R_{\rm vis} - R_{\rm miss}$ and E_γ is the energy of an isolated photon candidate, if one is identified. This selection has a somewhat lower efficiency and a larger radiative background, of 76% and 21%, respectively. Since it depends mainly on energy measurements in the detector, whereas the kinematic fit is more sensitive to measurements of jet directions, the two procedures for selecting non-radiative events are complementary and allow a systematic uncertainty to be evaluated.

We select 152 non-radiative events in the 130 GeV data sample and 139 in the 136 GeV sample using the kinematic fit. The mean centre-of-mass energy of the combined sample is approximately 133 GeV. Our alternative selection gives 155 and 142 events at 130 and 136 GeV, respectively, corresponding to the same centre-of-mass energy of the combined sample. Using Monte Carlo information, the total background from two-photon and tau pair events in the selected samples of non-radiative events is estimated to be less than 1%. Given the small numbers of events in our data samples, we therefore assume the influence of these backgrounds on our results to be negligible.

4.2 Corrections to observed distributions

The distributions of QCD observables are corrected for acceptance, the effects of detector resolution and the presence of radiative events. Each observable is evaluated using two samples of Monte Carlo events. The first includes full simulation of the OPAL detector and contains only those events which pass the cuts applied to the data (detector level). The second does not include initial state radiation or detector effects and allows all particles with lifetimes shorter than $3 \cdot 10^{-10}$ s to decay (hadron level). Both samples are generated at 130 GeV and 136 GeV. Distributions normalised to the number of events at the detector

and the hadron level are compared to derive bin-by-bin correction factors which are used to correct the observed distributions.

5 Event shapes

The properties of hadronic events may be characterised by a set of event shape observables. Each of these is calculated using all selected charged tracks and electromagnetic clusters. The following quantities are considered:

Thrust T: This observable is defined by the expression [10]

$$T = \max_{\vec{n}} \left(\frac{\sum_i |p_i \cdot \vec{n}|}{\sum_i |p_i|} \right) \quad . \tag{1}$$

The thrust axis $\vec{n}_T$ is the direction $\vec{n}$ which maximises the expression in parentheses. A plane through the origin and perpendicular to $\vec{n}_T$ divides the event into two hemispheres H_1 and H_2.

Thrust major T_{maj}: The maximisation in equation 1 is performed with the condition that $\vec{n}$ must lie in the plane perpendicular to $\vec{n}_T$. The resulting vector is called $\vec{n}_{T_{\mathrm{maj}}}$.

Thrust minor T_{min}: The expression in parentheses is evaluated for the vector $\vec{n}_{T_{\mathrm{min}}}$ which is perpendicular both to $\vec{n}_T$ and to $\vec{n}_{T_{\mathrm{maj}}}$.

Oblateness O: This observable is defined by $O = T_{\mathrm{maj}} - T_{\mathrm{min}}$ [11].

Sphericity S and Aplanarity A: These observables are based on the momentum tensor

$$S^{\alpha\beta} = \frac{\sum_i p_i^\alpha p_i^\beta}{\sum_i p_i^2} \quad , \quad \alpha, \beta = 1, 2, 3 \quad .$$

The three eigenvalues Q_j of $S^{\alpha\beta}$ are ordered such that $Q_1 < Q_2 < Q_3$. These then define S [12] and A [13] by

$$S = \frac{3}{2}(Q_1 + Q_2) \quad \text{and} \quad A = \frac{3}{2} Q_1 \quad .$$

C-parameter C: The momentum tensor $S^{\alpha\beta}$ is linearised to become

$$\Theta^{\alpha\beta} = \frac{\sum_i (p_i^\alpha p_i^\beta)/|p_i|}{\sum_i |p_i|} \quad , \quad \alpha, \beta = 1, 2, 3 \quad .$$

The three eigenvalues λ_j of this tensor define C [14] with

$$C = 3(\lambda_1\lambda_2 + \lambda_2\lambda_3 + \lambda_3\lambda_1) \quad .$$

Heavy Jet Mass M_H: The hemisphere invariant masses are calculated using the particles in the two hemispheres H_1 and H_2. We define M_H [15] as the heavier mass, divided by $\sqrt{s}$.

Jet Broadening variables B_T and B_W: These are defined by computing the quantity

$$B_k = \left(\frac{\sum_{i \in H_k} |p_i \times \vec{n}_T|}{2 \sum_i |p_i|} \right)$$

for each of the two event hemispheres, H_k, defined above. The two observables [16] are defined by

$$B_T = B_1 + B_2 \quad \text{and} \quad B_W = \max(B_1, B_2)$$

where B_T is the total and B_W is the wide jet broadening.

In the following, we use the symbol y to denote a generic event shape observable, where larger values of y indicate regions dominated by the radiation of hard gluons and small values of y indicate the region influenced by multiple soft gluon radiation. The quantities $1-T$, M_H, B_T and B_W are of special interest for quantitative QCD studies, because QCD calculations including the resummation of leading and next to leading logarithmic terms to all orders exist for these observables (NLLA calculations) [16,17].

Figures 1 and 2 show the distributions of the event shape observables $T_{\rm maj}$, $T_{\rm min}$, O, S, A and C, corrected for detector acceptance and initial state radiation. The data at 130 and 136 GeV are combined and then corrected using the combined samples of Monte Carlo events. The resulting data points are shown with the statistical and systematic uncertainties added in quadrature. The numerical values for all the event shape distributions are listed in Tables 1 to 5 together with the mean value for each observable.

The experimental systematic uncertainties are estimated by repeating the analysis with information from the charged tracks only and from electromagnetic clusters only. In each bin, the largest of the differences between the three sets of results is taken as a systematic error. We also repeat the analysis requiring $|\cos\theta_T| < 0.7$, which confines the events mostly to the barrel region of the detector, and take the deviation from the standard result as a systematic error. Uncertainties arising from the selection of non-radiative events are estimated by repeating the analysis using the selection based on visible energy and missing momentum and the difference relative to the standard result is taken as the systematic error. The total systematic error is taken as the sum in quadrature of these uncertainties.

The event shape distributions are compared with predictions from Monte Carlo simulations. We use PYTHIA 5.7, ARIADNE 4.06 [18], HERWIG 5.8 and COJETS 6.23 [19,20] for these simulations with parameters tuned to OPAL data at 91 GeV [5,20]. The general features of the event shape distributions are reasonably well described by the Monte Carlo models within the uncertainties of our data. A similar level of agreement is found for the $1-T$, M_H, B_T and B_W distributions which are shown in Figure 4 without Monte Carlo predictions. The COJETS model tends to give a slightly poorer description of the data than PYTHIA, ARIADNE or HERWIG.

6 Jet rates

The production of hadrons in jets is one of the characteristic features of hadronic production in high energy collisions. The rate of multi-jet production is intimately linked to the magnitude of the strong coupling constant α_s and the variation of the jet rates with energy provides a simple and intuitive illustration of the running of α_s. A number of different algorithms exist to group particles into jets. We consider the Durham [8] and JADE [21] recombination algorithms, and the cone jet finding algorithm [22].

Recombination jet finding algorithms. In recombination algorithms, the scaled invariant masses $y_{ij} = (M_{ij}/E_{\rm vis})^2$ are calculated between particles in an event[2], and particles with the smallest y_{ij} are combined into pseudoparticles. The pairing and combination of particles is repeated until all remaining pairings have a value of y_{ij} greater than some jet resolution $y_{\rm cut}$. The two recombination schemes which we consider differ in the definition of invariant mass M_{ij} between (pseudo-) particles.

JADE scheme (E0): The invariant mass is defined as $M_{ij}^2 = 2E_iE_j(1-\cos\theta_{ij})$ where E_i and E_j are the energies of particles i and j and $\cos\theta_{ij}$ is the angle between their 3-momentum vectors. We measure the relative number of n-jet events, R_n, as a function of the jet resolution $y_{\rm cut}$.

Durham scheme (D): In this case, M_{ij}^2 is replaced by $2\min(E_i^2, E_j^2)\cdot(1-\cos\theta_{ij})$ which is the effective transverse momentum between particles. We again compute the relative number of n-jet events as a function of $y_{\rm cut}$.

The JADE E0 scheme has been widely used by earlier experiments and therefore allows comparison with lower energy data. The Durham scheme is a more recent development and is particularly interesting because it allows the application of QCD NLLA calculations in regions of small $y_{\rm cut}$. As in previous analyses [24], we define the differential jet rate $D_2(y_{\rm cut}) \equiv dR_2(y_{\rm cut})/dy_{\rm cut}$, where R_2 is the two-jet rate, for performing fits to the data.

Cone algorithm. In the cone jet finding algorithm, a jet is defined as a set of collimated particles whose 3-momentum vectors lie inside a cone of half angle R, where the direction of the sum of their 3-momentum vectors defines the cone axis. In addition, the total energy of the particles assigned to a jet is required to exceed some minimum value ε. The cone half angle R and energy cutoff ε are the analogues of the jet resolution parameter $y_{\rm cut}$ in the E0 and D schemes, and typical values are $R = 0.7$ rad and $\varepsilon = 7$ GeV for jets in e^+e^- annihilation at LEP I energies. When analysing events at the detector level, we replace ε by $\varepsilon' = \varepsilon \cdot E_{\rm vis}/\sqrt{s}$ which compensates for the incomplete detection of the energy of the event. In our studies, the jet rate is computed at fixed $\varepsilon = 7$ GeV as R is varied, and at fixed $R = 0.7$ as ε is varied. The former is sensitive to the angular structure of jets, and the latter to their energy distribution.

[2] In this section $E_{\rm vis}$ is the sum of the energies of the particles considered for jet finding.

The same procedures as described in section 5 are followed to correct and combine the data and to evaluate systematic uncertainties. The jet rate distributions are shown in Figure 3 with numerical values given in Tables 6 to 9. The data points in each distribution are correlated between bins since all events enter in each bin of $y_{\rm cut}$, R or ε. The curves show the predictions from the PYTHIA Monte Carlo. Numerical values for the differential two-jet rate distribution using the Durham scheme, D_2, are given in Table 10.

With the E0 and the D schemes we observe a slight excess of the 3-jet rate, and a corresponding deficit of the 2-jet rate, compared to the Monte Carlo predictions. With the cone jet algorithm we find that the 3-jet rate agrees with the Monte Carlo predictions while there is a small excess of the 4-jet rate at the expense of the 2-jet rate.

7 Determination of α_s(133 GeV)

Our measurement of the strong coupling constant $\alpha_s(133\ \text{GeV})$ is based on fits of the QCD predictions to the corrected distributions for $1-T$, M_H, B_T, B_W and D_2 using the Durham jet scheme. The theoretical descriptions of these five observables are the most complete, allowing the use of combined $\mathcal{O}(\alpha_s^2)$+NLLA QCD calculations [16,17,23]. The large y regions of the event shape distributions are best described by $\mathcal{O}(\alpha_s^2)$ calculations, and the small y regions with NLLA predictions. In order to achieve the best description of the data over the largest range of y, the $\mathcal{O}(\alpha_s^2)$ and NLLA calculations are combined using a "matching scheme". We follow the procedures described in reference [24] as closely as possible in order to obtain results which we can compare directly to our previous analysis. In particular, we choose the $\ln(R)$-matching scheme, and fix the renormalisation scale parameter x_μ (defined by $\mu = x_\mu\sqrt{s}$, where μ is the energy scale at which the theory has been renormalised) to be 1.

The analytic QCD predictions are calculated in terms of integral, or cumulative, event shape distributions which are corrected for hadronisation effects by multiplying by the ratio of hadron and parton level integral distributions calculated by a Monte Carlo model. We use JETSET 7.4 to generate events at $\sqrt{s} = 133$ GeV for this purpose. The corrected integral distributions are converted to a differential distribution with the same binning as the data before being fitted.

The fit ranges are determined by the following considerations: the ratio between Monte Carlo event shape distributions computed for partons and hadrons should be close to unity to within about 10%; they should be similar to the fit ranges used in our analysis of our data at $\sqrt{s} = M_{\rm Z^0}$ [24] and distributions of partons from Monte Carlo models should be well described by the analytic predictions.

The fits are based on the χ^2 method, where we take the statistical errors on the fitted data points, including contributions from limited Monte Carlo statistics, into account. Our data are binned into a small number of wide bins so that we may safely neglect correlations arising from bin-to-bin migration.

We find satisfactory fits for all five observables with χ^2/d.o.f. of the fits generally of $\mathcal{O}(1)$. The results are shown in Table 11 and in Figure 4. We observe that for all

observables except B_W, the data points lie above the fit at larger y while they lie below the fit at smaller y. This is consistent with our observation in section 6 of a slight excess of 3-jet events and a slight deficit of 2-jet events.

The statistical uncertainties are quite large due to the small number of events in our data sample, and are estimated from the spread of α_s values derived from fits to a number of independent distributions. The small size of the data sample makes it impractical to divide it into subsets and fit these individually, however Monte Carlo distributions fluctuate in the same way as our data and therefore may be used to give an adequate estimate of the statistical uncertainty. We perform fits to ten independent sets of Monte Carlo distributions, each computed using on average the same number of events as in our data sample, and find the fractional error on α_s from the variance in the set of ten fitted α_s values.

Experimental uncertainties are studied as in section 5 by fitting distributions determined using only charged tracks or only electromagnetic clusters, with the alternative non-radiative selection, or with the thrust axis angle cut changed to $|\cos\theta_T| < 0.7$. The total experimental uncertainty is defined by the quadratic sum of: the largest difference between the central result and the results from tracks or clusters only; the difference found when using the alternative selection; and the difference from using $|\cos\theta_T| < 0.7$. The experimental uncertainties are shown in Table 11 and are about the same size as the statistical uncertainties.

Systematic effects connected with the correction of the QCD predictions for hadronisation effects are estimated using the methods described in detail in reference [24]. We:

- vary the hadronisation parameters σ_Q and b of our standard Monte Carlo, JETSET 7.4, by $\pm$ 1 standard deviation about their tuned values [5];

- change the minimum value Q_0 for the parton virtuality from its tuned value $Q_0 =$ 1.9 GeV to $Q_0 = 4$ GeV, which corresponds to a change of the mean parton multiplicity from 6.8 to 4.7;

- determine the hadronisation corrections using parton level distributions arising only from events where the initial quark-antiquark pair are light quarks (udsc);

- use different QCD Monte Carlo event generators, HERWIG 5.8 and ARIADNE 4.06, with parameters also tuned to OPAL data at LEP I.

The total hadronisation uncertainty is defined by adding in quadrature the larger of the changes in α_s observed when varying σ_Q and b in JETSET; the change observed with $Q_0 = 4$ GeV in JETSET; and both differences with respect to the standard result when we use HERWIG or ARIADNE. For all observables the hadronisation uncertainties are relatively small compared to the statistical or experimental errors. They are smaller than in our earlier analysis at $\sqrt{s} = M_{\mathrm{Z}^0}$, which may partly be due to improvements in the Monte Carlo models and their tunings, and partly due to the reduced influence of hadronisation effects at the higher centre-of-mass energy [25].

The significance of uncomputed higher order terms in the theory may be estimated by studying the effects of varying the renormalisation scale parameter x_μ. We estimate the dependence of our fit results on the renormalisation scale x_μ as in reference [24] by repeating the fits with $x_\mu = 0.5$ and $x_\mu = 2$. We find variations which are generally smaller than the statistical uncertainties and which are highly correlated between all observables.

The total errors for each individual observable are computed by adding in quadrature the statistical, the experimental, the hadronisation and the scale uncertainties. The total uncertainty on $\alpha_s(133\ \mathrm{GeV})$ is around 10% and the smallest error is given by the fit to B_W which has particularly small statistical and hadronisation uncertainties.

A combined result for the strong coupling strength at 133 GeV is derived from a weighted average as described in reference [24]. The statistical error of the combined result is estimated with ten independent samples of Monte Carlo events as for the individual measurements. Our final result is

$$\alpha_s(133\ \mathrm{GeV}) = 0.110 \pm 0.005(\mathrm{stat.}) \pm 0.009(\mathrm{syst.}) \quad .$$

This result is equivalent to $\alpha_s(M_{\mathrm{Z}^0}) = 0.116 \pm 0.010$. In comparison, our measurements at LEP I with a slightly larger set of observables based on $\mathcal{O}(\alpha_s^2)$+NLLA QCD calculations[3] yielded $\alpha_s(M_{\mathrm{Z}^0}) = 0.120 \pm 0.006$ [24]. In order to compare average α_s values using exactly the same theoretical predictions and observables, we compute the weighted average from our present fits to $1-T$, M_H, B_T and B_W which yields $\alpha_s(133\ \mathrm{GeV}) = 0.111 \pm 0.009$ ($\alpha_s(M_{\mathrm{Z}^0}) = 0.117 \pm 0.010$). Our previous analysis at $\sqrt{s} = M_{\mathrm{Z}^0}$ gave $\alpha_s(M_{\mathrm{Z}^0}) = 0.116 \pm 0.006$ from fits of the same predictions to the same variables. Our present determination of α_s is therefore consistent with our measurement at LEP I, and with other published measurements of α_s at $\sqrt{s} \approx 133$ GeV [26].

8 Inclusive charged particle measurements

One of the basic measurements in $\mathrm{e^+e^-}$ annihilations is that of the number and momenta of the charged particles produced. Data have been accumulated from centre-of-mass energies of around 10 GeV up to the most recent LEP energy of 136 GeV. According to the hypothesis of Local Parton Hadron Duality (LPHD) [27], the low energy particles produced in $\mathrm{e^+e^-}$ collisions are the remnants of the emission of many soft gluons and their distributions may be predicted in the context of the Leading Logarithmic Approximation (LLA). There are a number of variants of the LLA which differ in the integration methods used to compute higher order terms – the most widely used are the modified leading logarithmic approximation (MLLA) [27,28] and the next-to-leading logarithmic approximation (NLLA) [29]. For all the LLA predictions, the assumption of LPHD is invoked to predict distributions of hadrons. The calculations make specific predictions not only about the shapes of the distributions but also about their variation with energy. The comparison of the energy evolution of the data with the predictions therefore forms

[3]The $\mathcal{O}(\alpha_s^2)$+NLLA calculation fitted to D_2 in reference [24] has since been improved. We use the improved version [23] in this analysis.

an important test of the LLA approach to QCD calculations. Such a test is important as the LLA methods form the basis of many of the widely used QCD Monte Carlo event generators.

The distributions we study are:

Fragmentation functions: We scale the measured momenta p of the charged particles by the beam energy $E_{\rm beam}$ to define $x_p = p/E_{\rm beam}$ for each particle. We study the distribution of x_p, commonly referred to as the fragmentation function, which emphasises the higher momentum region, and also the logarithmic distribution of $\xi_p = \ln(1/x_p)$, which emphasises the low momentum region. The fragmentation function may be integrated to yield a measurement of the average charged multiplicity, $\langle n_{\rm ch} \rangle$, of the events.

Multiplicity distribution: We measure the distribution of the number of charged particles per event and derive several quantities that characterise the multiplicity distribution. In particular, we evaluate the mean charged multiplicity, $\langle n_{\rm ch} \rangle$, the dispersion $D = (\langle n_{\rm ch}^2 \rangle - \langle n_{\rm ch} \rangle^2)^{\frac{1}{2}}$, the ratio $\langle n_{\rm ch} \rangle / D$, the normalised second moment $C_2 = \langle n_{\rm ch}^2 \rangle / \langle n_{\rm ch} \rangle^2$ and the second binomial moment $\mathcal{R}_2 = \langle n_{\rm ch}(n_{\rm ch}-1) \rangle / \langle n_{\rm ch} \rangle^2$.

Rapidity distribution: We determine the rapidity, Y, of each charged particle with respect to the thrust axis. The rapidity is defined by $Y = \mid \ln(\frac{E+p_{||}}{E-p_{||}}) \mid$ where $p_{||}$ is the momentum component parallel to the thrust axis, and E the particle energy.

Projected momentum spectra: We measure the distributions of 3-momentum components parallel ($p_\perp^{\rm in}$) and perpendicular ($p_\perp^{\rm out}$) to the event plane, defined by the eigenvectors of the momentum tensor associated with the two largest eigenvalues.

The fragmentation functions, momentum spectra and rapidity distribution are corrected using the bin-by-bin method described in section 5. This correction method is not appropriate for the multiplicity distribution, since resolution and acceptance effects cause significant migration between bins. Instead, we follow the procedure used in our previous publication [30] and apply a matrix correction to correct for detector resolution effects, followed by a bin-by-bin correction which accounts for the effects due to acceptance cuts and residual initial state radiation. The distributions from the two data samples at 130 and 136 GeV are combined after the application of the corrections.

Systematic uncertainties are evaluated by repeating the analysis using the alternative selection for non-radiative events, or by requiring the thrust axis of the event to be within $|\cos\theta_T| < 0.7$. This eliminates events oriented towards the endcaps of the detector where the tracking performance is degraded by the reduced number of hits in the tracking chambers allowed by the geometry. Uncertainties associated with the selection of charged tracks are estimated by varying the track selection cuts and repeating the analysis (the largest contribution coming from varying the cut on the distance of tracks from the interaction region at the point of closest approach in r-ϕ). The differences relative to the standard analysis in each case are added in quadrature to define the systematic uncertainty.

The x_p and ξ_p distributions are shown in Figure 5 (with numerical values given in Tables 12 and 13), and the distributions of multiplicity, Y, $p_\perp^{\rm in}$, and $p_\perp^{\rm out}$ are shown in Figure 6 (numerical values given in Tables 14 and 15) . The predictions of several Monte Carlo models are also shown in the figures. The agreement of PYTHIA, HERWIG and ARIADNE is in general good for all distributions, whilst COJETS provides a poorer description of the data, especially of the rapidity distribution at low Y and the higher momentum regions of the $p_\perp^{\rm in}$ and $p_\perp^{\rm out}$ distributions. The errors on the multiplicity distribution are correlated from point-to-point due to the matrix correction, but there is evidence for a slight shift towards lower multiplicity relative to the distributions predicted by PYTHIA, ARIADNE and HERWIG. The multiplicity distribution above $\langle n_{\rm ch}\rangle = 16$ is not modelled well by COJETS. Distributions of ξ_p predicted by the models have not been shown for clarity, but nonetheless they are found to give a good description of the shape of the data.

8.1 Studies with the ξ_p distribution

The LLA is expected to be valid for particles with low scaled momenta ($x_p < 0.1$) and may be used to calculate the ξ_p distribution analytically. In the MLLA, the distribution is predicted to have a hump-backed shape which may asymptotically be approximated by a Gaussian function around the peak of the distribution [27, 28]. Calculation of the next order terms (NLLA) modify this shape to a skewed Gaussian [29]. The free parameters are, in each case, an effective QCD scale, a higher order correction and an energy-dependent normalisation. Figure 5 (b) shows fits of both Gaussian (LLA) and skewed Gaussian (NLLA) functions to the region within about one unit of ξ_p around the peak of the ξ_p distribution. The fitted functions have been extrapolated to the rest of the distribution. Both functions give a good fit to the peak region with a χ^2/d.o.f. of less than one. Kinematic effects become important in determining the momentum distribution at low ξ_p and the LLA approach is not expected to be reliable in this area of the distribution. However at large ξ_p where the emission of many very soft gluons plays an important role in determining the momentum distribution, the addition of higher order terms is seen to improve the description of the data by the LLA predictions.

The LLA predictions may be fitted to the ξ_p distribution measured at $\sqrt{s}$=91 GeV, determining the two energy-independent parameters, and then used to predict the shape of the distribution at higher energies. The parameters obtained from fits of the skewed Gaussian to the ξ_p distribution from Z^0 decays from our previous publication [31] are used, together with a free parameter for the normalisation, to fit the ξ_p distribution at 133 GeV. The resulting fit is good, with only a small increase in χ^2/d.o.f. compared to the fit with all three parameters free. This indicates that the LLA calculations predict the correct energy dependence for the shape of the ξ_p distribution around its peak.

The peak of the ξ_p distribution is determined from the fit of the skewed Gaussian and is found to be

$$\xi_0 = 3.94 \pm 0.05(\text{stat.}) \pm 0.11(\text{syst.}) \quad .$$

The systematic uncertainty is evaluated by repeating the analysis with the alternative selection, with $|\cos\theta_T| < 0.7$, by varying the fit range or by fitting a Gaussian function.

These contributions are listed in Table 16 and are added in quadrature to give the overall systematic error.

8.2 Charged multiplicity determination

We integrate the corrected and combined x_p distribution and find as our final result for the mean charged particle multiplicity at $\sqrt{s} = 133$ GeV

$$\langle n_{\rm ch} \rangle = 23.40 \pm 0.45(\text{stat.}) \pm 0.47(\text{syst.}) \quad .$$

The systematic uncertainty is estimated as for ξ_0 by repeating the analysis using the alternative selection or the more restrictive thrust axis angle cut and adding the differences in the corrected multiplicity values in quadrature. We also use the JETSET or HERWIG simulated event samples instead of PYTHIA for evaluating the corrections, determine $\langle n_{\rm ch} \rangle$ from the ξ_p distribution or integrate the uncorrected data distributions and apply correction factors to the results. In all cases, no significant change in the multiplicity is observed.

The mean charged multiplicity may also be determined from the corrected and combined multiplicity distribution shown in Figure 6. The result is $\langle n_{\rm ch} \rangle = 23.61 \pm 0.45(\text{stat.}) \pm 0.55(\text{syst.})$, which agrees very well with the measurement determined from the fragmentation function. The systematic uncertainty is estimated as described above and details are given in Table 16. An estimate of the model dependence of the correction procedure is given by the difference between values obtained when the data are corrected with the JETSET or HERWIG Monte Carlo models. As a further systematic check, $\langle n_{\rm ch} \rangle$ is evaluated by applying a simple correction factor to the measured value of $\langle n_{\rm ch} \rangle$: this correction is the ratio between the PYTHIA prediction without detector simulation or initial state radiation, to the prediction for $\langle n_{\rm ch} \rangle$ when these two effects are included. The change in the corrected value for $\langle n_{\rm ch} \rangle$ is small, nonetheless we include this difference as an estimate of the systematic error due to the unfolding process. The total systematic errors for both determinations of $\langle n_{\rm ch} \rangle$ are of comparable size, and we choose the $\langle n_{\rm ch} \rangle$ value determined from the integrated fragmentation function as our central value as the corrections for detector effects are simpler and the systematic uncertainty is slightly smaller.

The multiplicity distribution is also used to evaluate the dispersion and higher multiplicity moments. The results are

$$D = 7.63 \pm 0.35 \pm 0.46$$

$$\langle n_{\rm ch} \rangle / D = 3.10 \pm 0.13 \pm 0.12$$

$$C_2 = 1.104 \pm 0.009 \pm 0.008$$

$$\mathcal{R}_2 \ = 1.062 \pm 0.009 \pm 0.009$$

where in each case the first error is statistical and the second systematic. The systematic uncertainties are estimated in the same way as for $\langle n_{\rm ch} \rangle$ and are detailed in Table 16.

The predicted value of $\langle n_{\rm ch}\rangle$ from PYTHIA is 24.2, whilst HERWIG and ARIADNE both predict 24.1, all of which are slightly higher than the data. If the PYTHIA multiplicity distribution in Figure 6 is shifted down by half a unit, its shape is in good agreement with our data. COJETS, with its present tuning, predicts $\langle n_{\rm ch}\rangle$ in excess of 25. Other measurements of $\langle n_{\rm ch}\rangle$ and D at this energy [26,32] are consistent with our data.

9 Energy evolution

In this section we compare our results with data recorded at lower energies and compare to analytic QCD or Monte Carlo predictions. Figure 7 (a) shows our measurement of $\langle n_{\rm ch}\rangle$ compared to results at energies from 12 to 136 GeV [26,32,33]. The curve is a fit to the NLLA prediction for the evolution of the charged particle multiplicity [34] with energy,

$$\langle n_{\rm ch}\rangle = a\alpha_s(\sqrt{s},\Lambda)^b \exp(c/\sqrt{\alpha_s(\sqrt{s},\Lambda)})(1+\mathcal{O}(\sqrt{\alpha_s(\sqrt{s},\Lambda)})$$

in which a and Λ are free parameters and b and c are constants computed from the theory. The level of precision of the calculation is such that the first-order expression for α_s is appropriate and therefore Λ is an effective scale, not directly comparable to $\Lambda_{\overline{\rm MS}}$.

All data points between 12 and 133 GeV are fitted and the fit gives $\Lambda = 0.165 \pm 0.030$ GeV and $a = 0.070 \pm 0.005$ with χ^2/d.o.f.=0.54. The multiplicity value given by the fit at 133 GeV is 24.3 ± 0.2 where the error takes into account correlations between the fitted parameters. If the fit is performed excluding the 133 GeV data point, the expected value of $\langle n_{\rm ch}\rangle$ at 133 GeV is 24.4 ± 0.2 which is about one and a half standard deviations higher than our measured value. This may, however, be due to missing higher orders in the calculations, or simply to a statistical fluctuation in the data. It should also be noted that the NLLA function takes no account of the different quark flavour compositions at the different energies, and that charged particle multiplicities have been shown [35] to depend on the quark flavour composition. Monte Carlo models which include such effects predict charged particle multiplicities in the range 24.1–24.2 (section 8.2).

Figure 7 (b) presents our result for the position of the peak in the ξ_p distribution, ξ_0, compared with lower energy data [31,36,37]. The position of the peak ξ_0 as a function of centre-of-mass energy is predicted in the MLLA including sub-leading effects [28] to follow

$$\xi_0 = \tau(1/2 + \sqrt{C/\tau} - C/\tau) \qquad (2)$$

where $\tau = \ln(\sqrt{s}/2\Lambda)$, C is given by the theory and the single free parameter Λ is an effective QCD scale. This expression is equivalent to the NLLA formula given in reference [29] and predicts an almost linear variation of ξ_0 with $\ln(\sqrt{s})$.

The curve in Figure 7 (b) shows the result of a fit of equation 2 to the data from 14 to 133 GeV which yields a value of $\Lambda = 0.263 \pm 0.004$ GeV with a χ^2/d.o.f. of 5.6 which is dominated by contributions from the data points with small errors at 29 and 35 GeV. If these points are removed from the fit, the χ^2/d.o.f. falls to 1.1 and Λ is essentially unchanged. If the 133 GeV data point is excluded from the fit, the result is unchanged.

Our measurements of $\langle n_{\rm ch}\rangle/D$, C_2 and $\mathcal{R}_2$ are consistent within errors with the values determined at LEP I and lower energy [30,37] and imply that these quantities do not vary appreciably with energy.

Figure 8 (a) presents the 3-jet rate R_3 at fixed $y_{\rm cut} = 0.08$ compared with lower energy data [38]. The R_3 value at 133 GeV is somewhat high as might be expected from Figure 3, although there is a sizeable systematic uncertainty in this number. The curve is a fit to the data of a prediction from perturbative QCD [39] for the energy evolution of R_3 as described in reference [40]

$$R_3 = A\alpha_s(\sqrt{s}) + B\alpha_s^2(\sqrt{s}) \quad ,$$

where A and B are constants given by the theory. The 133 GeV data point is included in the fit which yields $\alpha_s(M_{\rm Z^0}) = 0.121 \pm 0.001$(stat.) with χ^2/d.o.f. = 1.1 (this changes to $\alpha_s(M_{\rm Z^0}) = 0.120$ if the new data are excluded from the fit).

The mean value of thrust, $\langle T\rangle$, measured at different centre-of-mass energies [24,26,41] is shown in Figure 8 (b). The predictions of several different Monte Carlo models are also shown. The energy evolution of $\langle T\rangle$ is fairly well described by the models within the measurement errors.

Finally we show in Figure 9 the value of the strong coupling constant α_s determined in different processes as a function of the energy scale Q. The measurements are listed in references [26,42], and references therein. In $\rm e^+e^-$ collisions the energy scale Q is usually taken to be $\sqrt{s}$. The α_s measurement shown at $Q = 1.8$ GeV is derived from τ decays where $Q = M_\tau$. The curve shows the second order QCD prediction for the running of α_s (with appropriate treatment of heavy quark production thresholds – see, for example, reference [42]) taking $\alpha_s(M_{\rm Z^0})$=0.120 as determined in reference [24]. Our measurement of α_s(133 GeV) is consistent with the running of α_s required by QCD.

10 Summary

We have presented in this paper a study of the properties of hadronic events produced with an effective centre-of-mass energy of 133 GeV. A large number of different event shape observables have been measured and compared with the predictions of Monte Carlo models. The description of the data by PYTHIA, HERWIG and ARIADNE with parameters tuned at $\rm Z^0$ energies is good in nearly all cases, whilst COJETS is somewhat less successful. The rate of jet production has also been studied and is broadly consistent with expectations.

From a fit of $\mathcal{O}(\alpha_s^2)$+NLLA QCD predictions to five event shape and jet rate distributions we determine $\alpha_s(133\ {\rm GeV}) = 0.110 \pm 0.005 \pm 0.009$. If this measurement is evolved to the $\rm Z^0$ mass it is equivalent to $\alpha_s(M_{\rm Z^0}) = 0.116 \pm 0.010$ which may be directly compared to our previous measurement of $\alpha_s(M_{\rm Z^0}) = 0.120 \pm 0.006$ using a very similar set of observables and $\mathcal{O}(\alpha_s^2)$+NLLA predictions.

The charged multiplicity has been determined to be $\langle n_{\rm ch}\rangle = 23.40 \pm 0.45 \pm 0.47$ which is about one and a half standard deviations lower than a fit of NLLA QCD to the lower

energy data. We have also determined the dispersion and second multiplicity moments, which are found to be consistent with the values determined at lower energies. The ξ_p distribution is well described by LLA calculations, and the position of the peak is measured to be $\xi_0 = 3.94 \pm 0.05 \pm 0.11$. This is in good agreement with the expectation for the energy evolution given by the LLA calculations.

Our studies show that most of the features of hadronic events produced in e^+e^- collisions at the currently accessible energies above the Z^0 mass are well described by QCD either in the form of analytic predictions or Monte Carlo models. Further tests of QCD at yet higher energies will soon be possible with the advent of the next phase of LEP.

Acknowledgements

We thank V.A. Khoze and B.R. Webber for valuable discussions concerning parts of this analysis. We particularly wish to thank the SL Division for the excellent start-up and performance of the LEP accelerator in the data taking run at centre-of-mass energies of 130-140 GeV and for their continuing close cooperation with our experimental group. In addition to the support staff at our own institutions we are pleased to acknowledge the
Department of Energy, USA,
National Science Foundation, USA,
Particle Physics and Astronomy Research Council, UK,
Natural Sciences and Engineering Research Council, Canada,
Israel Ministry of Science,
Israel Science Foundation, administered by the Israel Academy of Science and Humanities,
Minerva Gesellschaft,
Japanese Ministry of Education, Science and Culture (the Monbusho) and a grant under the Monbusho International Science Research Program,
German Israeli Bi-national Science Foundation (GIF),
Direction des Sciences de la Matière du Commissariat à l'Energie Atomique, France,
Bundesministerium für Bildung, Wissenschaft, Forschung und Technologie, Germany,
National Research Council of Canada,
Hungarian Foundation for Scientific Research, OTKA T-016660, and OTKA F-015089.

References

[1] OPAL Coll., K. Ahmet et al.: Nucl. Instrum. Methods A 305 (1991) 275

[2] OPAL Coll., G. Alexander et al.: Z. Phys. C 52 (1991) 175

[3] J. Allison et al.: Nucl. Instrum. Methods A 317 (1992) 47

[4] T. Sjöstrand: Comput. Phys. Commun. 82 (1994) 74

[5] OPAL Coll., G. Alexander et al.: CERN-PPE/95-126 (1995), Z. Phys. C (to be published)

[6] G. Marchesini et al.: Comput. Phys. Commun. 67 (1992) 465

[7] OPAL Coll., G. Alexander et al.: CERN-PPE/96-025 (1996), Sub. to Phys. Lett. B

[8] S. Catani et al.: Phys. Lett. B 269 (1991) 432

[9] OPAL Coll., M.Z. Akrawy et al.: Phys. Lett. B 236 (1990) 224

[10] S. Brandt et al.: Phys. Lett. 12 (1964) 57
E. Farhi: Phys. Rev. Lett. 39 (1977) 1587

[11] MARKJ Coll., D.P. Barber et al.: Phys. Rev. Lett. 43 (1979) 830

[12] J.D. Bjorken and S.J. Brodsky: Phys. Rev. D 1 (1970) 1416
SLAC-LBL Coll., G. Hanson et al.: Phys. Rev. Lett. 35 (1975) 1609

[13] S.L. Wu and G. Zobernig: Z. Phys. C 2 (1979) 107

[14] G. Parisi: Phys. Lett. B 74 (1978) 65
J.F. Donoghue, F.E. Low, and S.Y. Pi: Phys. Rev. D 20 (1979) 2759

[15] T. Chandramohan and L. Clavelli: Nucl. Phys. B 184 (1981) 365
L. Clavelli and D. Wyler: Phys. Lett. B 103 (1981) 383

[16] S. Catani, G. Turnock and B.R. Webber: Phys. Lett. B 295 (1992) 269

[17] S. Catani, L. Trentadue, G. Turnock and B.R. Webber: Nucl. Phys. B 407 (1993) 3

[18] L. Lönnblad: Comput. Phys. Commun. 71 (1992) 15

[19] R. Odorico: Comput. Phys. Commun. 32 (1984) 139
R. Odorico: Comput. Phys. Commun. 59 (1990) 527

[20] P. Mazzanti and R. Odorico: Nucl. Phys. B 394 (1993) 267

[21] JADE Coll., W. Bartel et al.: Z. Phys. C 33 (1986) 23

[22] OPAL Coll., R. Akers et al.: Z. Phys. C 63 (1994) 197

[23] G. Dissertori and M. Schmelling: Phys. Lett. B 361 (1995) 167

[24] OPAL Coll., P.D. Acton et al.: Z. Phys. C 59 (1993) 1

[25] Yu.L. Dokshitzer and B.R. Webber: Phys. Lett. B 352 (1995) 451

[26] L3 Coll., M. Acciarri et al.: CERN-PPE/95-192 (1995), Sub. to Phys. Lett. B

[27] Yu.L. Dokshitzer, V.A. Khoze, A.H. Mueller and S.I. Troyan: Basics of perturbative QCD. Editions Frontieres 1991

[28] V.A.Khoze Yu.L. Dokshitzer and S.I.Troyan: Int. J. Mod. Phys. A 7 (1992) 1875

[29] C.P. Fong and B.R. Webber: Nucl. Phys. B 355 (1991) 54

[30] OPAL Coll., P.D. Acton et al.: Z. Phys. C 53 (1992) 539

[31] OPAL Coll., M.Z. Akrawy et al.: Phys. Lett. B 247 (1990) 617

[32] DELPHI Coll., P. Abreu et al.: CERN-PPE/96-05 (1996), Sub. to Phys. Lett. B

[33] JADE Coll., W. Bartel et al.: Z. Phys. C 20 (1983) 187
PLUTO Coll., C. Berger et al.: Phys. Lett. B 95 (1980) 313
TASSO Coll., W. Braunschweig et al.: Z. Phys. C 45 (1989) 193
TPC Coll., H. Aihara et al.: Phys. Lett. B 134 (1987) 299
HRS Coll., M. Derrick et al.: Phys. Rev. D 34 (1986) 3304
AMY Coll., H.W. Zheng et al.: Phys. Rev. D 42 (1990) 737
ALEPH Coll., D. Decamp et al.: Phys. Lett. B 273 (1991) 181
DELPHI Coll., P. Abreu et al.: Z. Phys. C 50 (1991) 185
L3 Coll., B. Adeva et al.: Z. Phys. C 55 (1992) 39
OPAL Coll., R. Akers et al.: Z. Phys. C 68 (1995) 203

[34] B.R. Webber: Phys. Lett. B 143 (1984) 501

[35] OPAL Coll., R. Akers et al.: Phys. Lett. B 352 (1995) 176

[36] TASSO Coll., W. Braunschweig et al.: Z. Phys. C 47 (1990) 187
MARK II Coll., A. Petersen et al.: Phys. Rev. D 37 (1988) 1
TPC Coll., H. Aihara et al.: LBL-23727 (1988)
AMY Coll., Y.K. Li et al.: Phys. Rev. D 411 (1990) 2675
ALEPH Coll., D. Buskulik et al.: Z. Phys. C 55 (1992) 209
DELPHI Coll., P. Abreu et al.: Phys. Lett. B 275 (1992) 231
L3 Coll., B. Adeva et al.: Phys. Lett. B 229 (1991) 199

[37] M. Schmelling: Phys. Scripta 51 (1995) 683

[38] JADE Coll., S. Bethke et al.: Phys. Lett. B 213 (1988) 235
JADE Coll., W. Bartel et al.: Z. Phys. C 33 (1986) 23
MARK II Coll., S. Bethke et al.: Z. Phys. C 43 (1989) 325
MARK II Coll., G.S. Abrams et al.: Phys. Rev. Lett. 63 (1989) 1558
TASSO Coll., W. Braunschweig et al.: Phys. Lett. B 214 (1988) 286
AMY Coll., I.H. Park et al.: Phys. Rev. Lett. 62 (1989) 1713
L3 Coll., B. Adeva et al.: Phys. Lett. B 248 (1990) 464
OPAL Coll., M.Z. Akrawy et al.: Z. Phys. C 49 (1991) 375

[39] S. Bethke, Z. Kunszt, D.E. Soper and W.J. Stirling: Nucl. Phys. B 370 (1992) 310

[40] OPAL Coll., M.Z. Akrawy et al.: Phys. Lett. B 235 (1990) 389

[41] TASSO Coll., W. Braunschweig et al.: Z. Phys. C 47 (1990) 187
AMY Coll., Y.K. Li et al.: Phys. Rev. D 41 (1990) 2675
ALEPH Coll., D. Buskulic et al.: Z. Phys. C 55 (1992) 209
DELPHI Coll., D. Aarnio et al.: Phys. Lett. B 240 (1990) 271
L3 Coll., B. Adeva et al.: Z. Phys. C 55 (1992) 39

[42] S. Bethke: Nucl. Phys. (Proc. Suppl.) B 39 (1995) 198

Tables

T_{maj}	$1/\sigma \ \mathrm{d}\sigma/\mathrm{d}T_{\mathrm{maj}}$
0.00 - 0.04	$0.20 \pm 0.15 \pm 0.20$
0.04 - 0.08	$6.3 \pm 0.83 \pm 0.58$
0.08 - 0.12	$5.6 \pm 0.68 \pm 0.64$
0.12 - 0.16	$2.6 \pm 0.47 \pm 0.36$
0.16 - 0.22	$2.08 \pm 0.35 \pm 0.28$
0.22 - 0.30	$1.59 \pm 0.28 \pm 0.49$
0.30 - 0.40	$0.93 \pm 0.19 \pm 0.23$
0.40 - 0.50	$0.46 \pm 0.12 \pm 0.12$
0.50 - 0.60	$0.20 \pm 0.08 \pm 0.04$
mean value	$0.174 \pm 0.008 \pm 0.005$

T_{min}	$1/\sigma \ \mathrm{d}\sigma/\mathrm{d}T_{\mathrm{min}}$
0.00 - 0.04	$2.52 \pm 0.48 \pm 0.58$
0.04 - 0.06	$15.9 \pm 1.8 \pm 1.9$
0.06 - 0.08	$9.9 \pm 1.3 \pm 2.9$
0.08 - 0.10	$7.4 \pm 1.1 \pm 0.9$
0.10 - 0.12	$4.4 \pm 0.9 \pm 1.5$
0.12 - 0.14	$2.8 \pm 0.7 \pm 1.5$
0.14 - 0.16	$2.01 \pm 0.60 \pm 0.91$
0.16 - 0.20	$0.79 \pm 0.26 \pm 0.39$
0.20 - 0.24	$0.29 \pm 0.18 \pm 0.12$
0.24 - 0.30	$0.19 \pm 0.15 \pm 0.15$
mean value	$0.0801 \pm 0.0026 \pm 0.0017$

Table 1: Measured values for the T_{maj} and T_{min} distributions. The mean value of each observable is also shown. The first error is statistical, the second systematic.

O	$1/\sigma \ \mathrm{d}\sigma/\mathrm{d}O$
0.00 - 0.05	$9.43 \pm 0.83 \pm 0.60$
0.05 - 0.10	$3.87 \pm 0.52 \pm 0.57$
0.10 - 0.15	$2.31 \pm 0.43 \pm 0.67$
0.15 – 0.20	$1.76 \pm 0.39 \pm 0.29$
0.20 – 0.25	$1.00 \pm 0.27 \pm 0.37$
0.25 – 0.30	$0.59 \pm 0.20 \pm 0.16$
0.30 – 0.40	$0.33 \pm 0.10 \pm 0.14$
0.40 – 0.50	$0.15 \pm 0.07 \pm 0.05$
mean value	$0.094 \pm 0.006 \pm 0.003$

S	$1/\sigma \ \mathrm{d}\sigma/\mathrm{d}S$
0.00 - 0.02	$22.2 \pm 1.9 \pm 1.8$
0.02 - 0.04	$7.4 \pm 1.2 \pm 1.6$
0.04 - 0.06	$4.2 \pm 0.9 \pm 1.4$
0.06 - 0.12	$1.78 \pm 0.35 \pm 0.81$
0.12 - 0.20	$1.02 \pm 0.23 \pm 0.53$
0.20 - 0.30	$0.68 \pm 0.17 \pm 0.32$
0.30 - 0.50	$0.28 \pm 0.07 \pm 0.10$
0.50 - 0.70	$0.07 \pm 0.04 \pm 0.04$
mean value	$0.082 \pm 0.008 \pm 0.053$

Table 2: Measured values for the O and S distributions. The mean value of each observable is also shown. The first error is statistical, the second systematic.

A	$1/\sigma \ \mathrm{d}\sigma/\mathrm{d}A$
0.000 - 0.005	$112.0 \pm 8.7 \pm 6.1$
0.005 - 0.010	$41.3 \pm 5.8 \pm 4.9$
0.010 - 0.015	$15.3 \pm 3.5 \pm 5.45$
0.015 - 0.025	$9.6 \pm 2.0 \pm 4.2$
0.025 - 0.040	$2.4 \pm 0.8 \pm 1.0$
0.040 - 0.070	$0.62 \pm 0.33 \pm 0.49$
0.070 - 0.100	$0.21 \pm 0.21 \pm 0.41$
mean value	$0.0088 \pm 0.0009 \pm 0.0009$

C	$1/\sigma \ \mathrm{d}\sigma/\mathrm{d}C$
0.00 - 0.05	$0.54 \pm 0.18 \pm 0.43$
0.05 - 0.08	$5.6 \pm 0.9 \pm 1.6$
0.08 - 0.11	$4.9 \pm 0.8 \pm 1.3$
0.11 - 0.14	$3.02 \pm 0.58 \pm 0.43$
0.14 - 0.18	$2.24 \pm 0.43 \pm 0.72$
0.18 - 0.22	$1.79 \pm 0.39 \pm 0.44$
0.22 - 0.30	$1.04 \pm 0.22 \pm 0.21$
0.30 - 0.40	$1.15 \pm 0.22 \pm 0.15$
0.40 - 0.50	$0.60 \pm 0.15 \pm 0.26$
0.50 - 0.60	$0.69 \pm 0.16 \pm 0.24$
0.60 - 0.75	$0.48 \pm 0.11 \pm 0.11$
0.75 - 1.00	$0.08 \pm 0.03 \pm 0.04$
mean value	$0.254 \pm 0.013 \pm 0.008$

Table 3: Measured values for the A and C distributions. The mean value of each observable is also shown. The first error is statistical, the second systematic.

T	$1/\sigma \ \mathrm{d}\sigma/\mathrm{d}T$
0.70 – 0.78	$0.53 \pm 0.15 \pm 0.10$
0.78 – 0.85	$1.16 \pm 0.25 \pm 0.33$
0.85 – 0.88	$1.64 \pm 0.45 \pm 0.68$
0.88 – 0.91	$2.40 \pm 0.55 \pm 0.69$
0.91 – 0.93	$3.68 \pm 0.83 \pm 0.67$
0.93 – 0.95	$4.5 \pm 0.9 \pm 0.9$
0.95 – 0.96	$7.5 \pm 1.7 \pm 2.2$
0.96 – 0.97	$9.7 \pm 1.8 \pm 3.4$
0.97 – 0.98	$15.6 \pm 2.3 \pm 4.5$
0.98 – 0.99	$23.6 \pm 3.1 \pm 4.3$
0.99 – 1.00	$3.1 \pm 1.0 \pm 1.6$
mean value	$0.935 \pm 0.004 \pm 0.002$

M_H	$1/\sigma \ \mathrm{d}\sigma/\mathrm{d}M_H$
0.060 – 0.075	$0.50 \pm 0.23 \pm 0.20$
0.075 – 0.090	$1.93 \pm 0.51 \pm 0.78$
0.090 – 0.110	$5.04 \pm 0.90 \pm 1.07$
0.110 – 0.140	$6.89 \pm 0.95 \pm 0.96$
0.140 – 0.170	$4.85 \pm 0.78 \pm 1.20$
0.170 – 0.200	$3.46 \pm 0.67 \pm 0.33$
0.200 – 0.250	$2.20 \pm 0.42 \pm 0.37$
0.250 – 0.300	$1.82 \pm 0.38 \pm 0.49$
0.300 – 0.350	$2.11 \pm 0.41 \pm 0.77$
0.350 – 0.450	$0.76 \pm 0.17 \pm 0.14$
0.450 – 0.600	$0.14 \pm 0.06 \pm 0.05$
mean value	$0.205 \pm 0.007 \pm 0.006$

Table 4: Measured values for the T and M_H distributions. The mean value of each observable is also shown. The first error is statistical, the second systematic.

B_T	$1/\sigma \ \mathrm{d}\sigma/\mathrm{d}B_T$
0.000 – 0.030	$0.43 \pm 0.27 \pm 0.56$
0.030 – 0.040	$8.3 \pm 2.0 \pm 3.0$
0.040 – 0.050	$14.3 \pm 2.5 \pm 2.2$
0.050 – 0.060	$12.3 \pm 2.1 \pm 3.6$
0.060 – 0.075	$8.0 \pm 1.3 \pm 2.8$
0.075 – 0.090	$5.6 \pm 1.1 \pm 2.3$
0.090 – 0.110	$4.5 \pm 0.9 \pm 1.9$
0.110 – 0.130	$3.5 \pm 0.8 \pm 1.2$
0.130 – 0.160	$2.9 \pm 0.6 \pm 1.1$
0.160 – 0.200	$2.08 \pm 0.42 \pm 0.36$
0.200 – 0.250	$1.46 \pm 0.33 \pm 0.58$
0.250 – 0.300	$0.76 \pm 0.22 \pm 0.28$
0.300 – 0.350	$0.06 \pm 0.10 \pm 0.10$
mean value	$0.104 \pm 0.004 \pm 0.003$

B_W	$1/\sigma \ \mathrm{d}\sigma/\mathrm{d}B_W$
0.000 – 0.020	$2.81 \pm 0.80 \pm 0.55$
0.020 – 0.030	$16.1 \pm 2.6 \pm 0.6$
0.030 – 0.040	$15.0 \pm 2.2 \pm 2.6$
0.040 – 0.050	$10.2 \pm 1.8 \pm 2.3$
0.050 – 0.065	$8.4 \pm 1.4 \pm 1.1$
0.065 – 0.080	$4.6 \pm 1.0 \pm 1.0$
0.080 – 0.100	$3.6 \pm 0.8 \pm 1.7$
0.100 – 0.150	$3.42 \pm 0.52 \pm 0.47$
0.150 – 0.200	$1.24 \pm 0.29 \pm 0.22$
0.200 – 0.250	$0.56 \pm 0.19 \pm 0.31$
0.250 – 0.300	$0.10 \pm 0.10 \pm 0.12$
mean value	$0.073 \pm 0.003 \pm 0.003$

Table 5: Measured values for the B_T and B_W distributions. The mean value of each observable is also shown. The first error is statistical, the second systematic.

y_{cut}	R_2	R_3	R_4	R_5
0.005	$19.6 \pm 2.3 \pm 1.5$	$41.9 \pm 2.9 \pm 7.3$	$28.0 \pm 2.6 \pm 6.8$	$10.5 \pm 1.8 \pm 2.1$
0.009	$28.8 \pm 2.7 \pm 2.7$	$46.7 \pm 2.9 \pm 3.4$	$20.4 \pm 2.4 \pm 5.3$	$4.2 \pm 1.2 \pm 2.0$
0.013	$36.0 \pm 2.8 \pm 2.2$	$49.1 \pm 2.9 \pm 2.7$	$13.3 \pm 2.0 \pm 2.4$	$1.6 \pm 0.7 \pm 0.8$
0.020	$47.6 \pm 2.9 \pm 2.8$	$46.6 \pm 2.9 \pm 2.9$	$5.5 \pm 1.3 \pm 1.9$	$0.3 \pm 0.3 \pm 0.3$
0.030	$56.8 \pm 2.9 \pm 2.5$	$39.5 \pm 2.9 \pm 2.1$	$3.7 \pm 1.1 \pm 1.4$	–
0.040	$63.5 \pm 2.8 \pm 3.1$	$33.8 \pm 2.8 \pm 2.7$	$2.7 \pm 0.9 \pm 1.8$	–
0.050	$70.5 \pm 2.7 \pm 2.3$	$27.8 \pm 2.6 \pm 2.4$	$1.7 \pm 0.8 \pm 1.5$	–
0.060	$75.0 \pm 2.5 \pm 2.2$	$24.2 \pm 2.5 \pm 2.5$	$0.8 \pm 0.5 \pm 0.5$	–
0.070	$77.7 \pm 2.4 \pm 1.7$	$21.6 \pm 2.4 \pm 1.7$	$0.6 \pm 0.5 \pm 0.4$	–
0.080	$80.1 \pm 2.3 \pm 3.1$	$19.8 \pm 2.3 \pm 3.0$	–	–
0.095	$83.2 \pm 2.2 \pm 5.1$	$16.6 \pm 2.2 \pm 5.2$	–	–
0.115	$86.7 \pm 2.0 \pm 3.1$	$13.3 \pm 2.0 \pm 3.1$	–	–
0.135	$89.1 \pm 1.8 \pm 1.6$	$10.9 \pm 1.8 \pm 1.6$	–	–
0.160	$92.9 \pm 1.5 \pm 1.2$	$7.1 \pm 1.5 \pm 1.2$	–	–
0.188	$95.3 \pm 1.2 \pm 0.9$	$4.7 \pm 1.2 \pm 0.9$	–	–

Table 6: Measured values (in %) for the jet rates using the Jade E0 scheme. The first error is statistical, the second systematic.

$y_{\rm cut}$	R_2	R_3	R_4	R_5
0.0008	$16.7 \pm 2.2 \pm 2.1$	$27.9 \pm 2.6 \pm 6.4$	$27.8 \pm 2.6 \pm 4.3$	$27.5 \pm 2.6 \pm 4.7$
0.0013	$28.6 \pm 2.6 \pm 1.4$	$34.3 \pm 2.8 \pm 3.6$	$25.3 \pm 2.5 \pm 2.7$	$11.9 \pm 1.9 \pm 3.2$
0.0023	$39.7 \pm 2.9 \pm 5.2$	$38.0 \pm 2.8 \pm 3.8$	$14.8 \pm 2.1 \pm 2.0$	$7.6 \pm 1.6 \pm 2.7$
0.0040	$48.5 \pm 2.9 \pm 3.5$	$36.7 \pm 2.8 \pm 4.8$	$11.4 \pm 1.9 \pm 3.6$	$3.4 \pm 1.1 \pm 1.5$
0.0070	$58.7 \pm 2.9 \pm 4.2$	$34.6 \pm 2.8 \pm 4.7$	$5.8 \pm 1.4 \pm 1.8$	$0.9 \pm 0.5 \pm 0.9$
0.012	$66.2 \pm 2.8 \pm 1.0$	$30.4 \pm 2.7 \pm 1.1$	$2.7 \pm 1.0 \pm 1.0$	$0.7 \pm 0.5 \pm 0.8$
0.023	$71.9 \pm 2.6 \pm 4.3$	$27.4 \pm 2.6 \pm 5.3$	$0.7 \pm 0.5 \pm 1.3$	–
0.04	$81.7 \pm 2.3 \pm 2.0$	$18.0 \pm 2.3 \pm 2.3$	$0.3 \pm 0.3 \pm 0.6$	–
0.07	$90.2 \pm 1.7 \pm 3.3$	$9.8 \pm 1.7 \pm 3.3$	–	–
0.13	$95.3 \pm 1.2 \pm 3.4$	$4.7 \pm 1.2 \pm 3.4$	–	–
0.24	$99.6 \pm 0.4 \pm 1.3$	$0.4 \pm 0.4 \pm 1.3$	–	–
0.40	$100.0 \pm 0.0 \pm 0.0$	–	–	–

Table 7: Measured values (in %) for the jet rates using the Durham scheme. The first error is statistical, the second systematic.

R	R_2	R_3	R_4
0.3	$51.8 \pm 2.9 \pm 2.8$	$31.1 \pm 2.7 \pm 1.9$	$17.1 \pm 2.2 \pm 1.2$
0.5	$58.5 \pm 2.9 \pm 3.4$	$30.4 \pm 2.7 \pm 3.5$	$11.0 \pm 1.8 \pm 0.7$
0.7	$70.0 \pm 2.7 \pm 4.1$	$23.0 \pm 2.4 \pm 4.5$	$7.0 \pm 1.5 \pm 2.2$
0.9	$72.9 \pm 2.6 \pm 4.0$	$24.2 \pm 2.5 \pm 3.5$	$2.8 \pm 1.0 \pm 1.4$
1.1	$83.9 \pm 2.1 \pm 2.7$	$15.1 \pm 2.1 \pm 2.4$	$0.9 \pm 0.7 \pm 1.1$
1.3	$93.2 \pm 1.5 \pm 2.0$	$6.8 \pm 1.5 \pm 2.0$	–
1.5	$98.9 \pm 0.6 \pm 1.3$	$1.1 \pm 0.6 \pm 1.3$	–

Table 8: Measured values (in %) for the jet rates using the Cone algorithm as a function of the cone size R. The minimum jet energy ε is fixed at 7 GeV. The first error is statistical, the second systematic.

ε (GeV)	R_2	R_3	R_4
2	$50.7 \pm 2.9 \pm 4.1$	$32.6 \pm 2.7 \pm 4.9$	$16.8 \pm 2.2 \pm 1.3$
6	$67.9 \pm 2.7 \pm 2.2$	$24.6 \pm 2.5 \pm 3.3$	$7.5 \pm 1.5 \pm 1.2$
10	$74.1 \pm 2.5 \pm 2.8$	$21.9 \pm 2.4 \pm 3.8$	$4.0 \pm 1.1 \pm 1.4$
14	$78.6 \pm 2.4 \pm 6.1$	$19.5 \pm 2.3 \pm 6.1$	$1.9 \pm 0.8 \pm 0.7$
18	$80.3 \pm 2.3 \pm 3.8$	$18.9 \pm 2.3 \pm 4.0$	$0.8 \pm 0.5 \pm 1.0$
22	$88.0 \pm 1.9 \pm 2.8$	$11.4 \pm 1.8 \pm 3.4$	$0.5 \pm 0.4 \pm 0.9$
25.5	$92.1 \pm 1.6 \pm 4.6$	$7.8 \pm 1.6 \pm 4.8$	$0.1 \pm 0.1 \pm 0.2$

Table 9: Measured values (in %) for the jet rates using the Cone algorithm as a function of the minimum jet energy ε. The cone size R is fixed at 0.7 radians. The first error is statistical, the second systematic.

$y_{\rm cut}$	D_2	$y_{\rm cut}$	D_2
0.0003–0.0008	$286 \pm 52 \pm 50$	0.0120–0.0225	$5.1 \pm 1.4 \pm 4.0$
0.0008–0.0013	$216 \pm 41 \pm 39$	0.0225–0.0400	$5.6 \pm 1.1 \pm 2.3$
0.0013–0.0023	$113 \pm 20 \pm 37$	0.0400–0.0700	$2.85 \pm 0.63 \pm 0.73$
0.0023–0.0040	$53 \pm 11 \pm 22$	0.0700–0.1300	$0.86 \pm 0.23 \pm 0.14$
0.0040–0.0070	$33.7 \pm 6.2 \pm 4.6$	0.1300–0.2350	$0.40 \pm 0.13 \pm 0.24$
0.0070–0.0120	$15.5 \pm 3.4 \pm 6.1$	0.2350–0.4000	$0.026 \pm 0.027 \pm 0.078$

Table 10: Measured values for the differential two-jet rate D_2, using the Durham jet finding algorithm. The first error is statistical, the second systematic.

	$1-T$	M_H	B_T	B_W	D_2
$\alpha_s(133\ \text{GeV})$	**0.1213**	**0.1121**	**0.1114**	**0.1025**	**0.1042**
fit range	$0.05-0.3$	$0.17-0.45$	$0.075-0.25$	$0.05-0.2$	$0.004-0.235$
χ^2/d.o.f.	5.3/5	6.9/4	4.6/5	5.3/4	14/6
Statistical	$\pm$0.0074	$\pm$0.0071	$\pm$0.0059	$\pm$0.0043	$\pm$0.0045
tracks only	+0.0024	−0.0005	−0.0073	+0.0042	−0.0016
cluster only	+0.0001	−0.0014	−0.0007	+0.0017	+0.0014
$\cos\theta_T < 0.7$	0.0000	+0.0008	+0.0024	+0.0031	+0.0014
alt. sel.	+0.0011	+0.0067	+0.0038	+0.0041	+0.0093
Experimental Syst.	$\pm$0.0027	$\pm$0.0069	$\pm$0.0086	$\pm$0.0066	$\pm$0.0098
$b+1$ s.d.	+0.0004	+0.0004	+0.0003	+0.0005	−0.0001
$b-1$ s.d.	−0.0001	−0.0001	−0.0002	+0.0003	+0.0003
σ_q+1 s.d.	−0.0002	−0.0002	−0.0002	+0.0001	+0.0003
σ_q-1 s.d.	+0.0003	+0.0001	+0.0003	+0.0004	+0.0003
$Q_0 = 4$ GeV	−0.0004	+0.0009	−0.0009	+0.0006	+0.0021
udsc only	+0.0009	+0.0002	+0.0019	+0.0015	+0.0018
HERWIG 5.8	−0.0007	+0.0014	−0.0019	−0.0006	−0.0003
ARIADNE 4.06	+0.0010	−0.0014	+0.0012	+0.0004	0.0000
Total hadronisation	$\pm$0.0017	$\pm$0.0023	$\pm$0.0031	$\pm$0.0018	$\pm$0.0028
$x_\mu = 0.5$	−0.0058	−0.0039	−0.0055	−0.0034	−0.0006
$x_\mu = 2$	+0.0073	+0.0052	+0.0067	+0.0043	+0.0024
Total error	**$\pm$0.0104**	**$\pm$0.0111**	**$\pm$0.0125**	**$\pm$0.0089**	**$\pm$0.0113**

Table 11: Systematic errors on the value of $\alpha_s(133\ \text{GeV})$ derived using the $\mathcal{O}(\alpha_s^2)$+NLLA QCD calculations with $x_\mu = 1$. The $\ln(R)$-matching scheme is used throughout. Where a signed value is quoted, this indicates the direction in which $\alpha_s(133\ \text{GeV})$ changed with respect to the default analysis when a particular feature of the analysis is changed.

x_p	$1/\sigma \ \mathrm{d}\sigma_{\mathrm{ch}}/\mathrm{d}x_p$	x_p	$1/\sigma \ \mathrm{d}\sigma_{\mathrm{ch}}/\mathrm{d}x_p$
0.00 – 0.01	$616 \pm 17 \pm 13$	0.12 – 0.14	$27.9 \pm 2.4 \pm 0.5$
0.01 – 0.02	$449 \pm 13 \pm 22$	0.14 – 0.16	$20.0 \pm 2.0 \pm 0.3$
0.02 – 0.03	$268 \pm 10 \pm 9$	0.16 – 0.18	$15.2 \pm 1.8 \pm 1.1$
0.03 – 0.04	$176.5 \pm 8.3 \pm 4.8$	0.18 – 0.20	$12.3 \pm 1.6 \pm 1.2$
0.04 – 0.05	$141.2 \pm 7.5 \pm 6.9$	0.20 – 0.25	$9.0 \pm 0.9 \pm 0.1$
0.05 – 0.06	$106.8 \pm 6.5 \pm 3.7$	0.25 – 0.30	$4.9 \pm 0.6 \pm 0.6$
0.06 – 0.07	$81.7 \pm 5.6 \pm 4.3$	0.30 – 0.40	$2.6 \pm 0.3 \pm 0.2$
0.07 – 0.08	$65.6 \pm 5.1 \pm 3.2$	0.40 – 0.50	$0.95 \pm 0.19 \pm 0.1$
0.08 – 0.09	$56.7 \pm 4.7 \pm 3.0$	0.50 – 0.60	$0.48 \pm 0.13 \pm 0.01$
0.09 – 0.10	$42.8 \pm 4.1 \pm 1.1$	0.60 – 0.80	$0.23 \pm 0.06 \pm 0.02$
0.10 – 0.12	$35.3 \pm 2.7 \pm 1.7$	mean value	$0.052 \pm 0.001 \pm 0.001$

Table 12: Measured values for the x_p distribution (fragmentation function).The first error is statistical, the second systematic.

ξ_p	$1/\sigma \ \mathrm{d}\sigma_{\mathrm{ch}}/\mathrm{d}\xi_p$	ξ_p	$1/\sigma \ \mathrm{d}\sigma_{\mathrm{ch}}/\mathrm{d}\xi_p$
0.2 – 0.4	$0.13 \pm 0.04 \pm 0.03$	3.2 – 3.4	$6.40 \pm 0.35 \pm 0.12$
0.4 – 0.6	$0.23 \pm 0.07 \pm 0.08$	3.4 – 3.6	$6.24 \pm 0.35 \pm 0.30$
0.6 – 0.8	$0.19 \pm 0.06 \pm 0.04$	3.6 – 3.8	$6.88 \pm 0.37 \pm 0.46$
0.8 – 1.0	$0.72 \pm 0.12 \pm 0.01$	3.8 – 4.0	$6.46 \pm 0.35 \pm 0.08$
1.0 – 1.2	$0.95 \pm 0.14 \pm 0.04$	4.0 – 4.2	$6.35 \pm 0.35 \pm 0.38$
1.2 – 1.4	$1.27 \pm 0.16 \pm 0.17$	4.2 – 4.4	$6.70 \pm 0.36 \pm 0.54$
1.4 – 1.6	$2.12 \pm 0.21 \pm 0.04$	4.4 – 4.6	$6.17 \pm 0.34 \pm 0.21$
1.6 – 1.8	$2.56 \pm 0.23 \pm 0.13$	4.6 – 4.8	$5.66 \pm 0.33 \pm 0.12$
1.8 – 2.0	$2.98 \pm 0.25 \pm 0.18$	4.8 – 5.0	$5.78 \pm 0.33 \pm 0.29$
2.0 – 2.2	$3.40 \pm 0.26 \pm 0.17$	5.0 – 5.2	$4.94 \pm 0.31 \pm 0.21$
2.2 – 2.4	$4.14 \pm 0.29 \pm 0.18$	5.2 – 5.4	$3.68 \pm 0.26 \pm 0.23$
2.4 – 2.6	$4.80 \pm 0.31 \pm 0.13$	5.4 – 5.6	$3.09 \pm 0.25 \pm 0.19$
2.6 – 2.8	$5.36 \pm 0.32 \pm 0.28$	5.6 – 5.8	$2.41 \pm 0.23 \pm 0.18$
2.8 – 3.0	$5.92 \pm 0.34 \pm 0.29$	5.8 – 6.0	$1.66 \pm 0.21 \pm 0.07$
3.0 – 3.2	$6.10 \pm 0.35 \pm 0.23$	6.0 – 6.2	$0.89 \pm 0.31 \pm 0.43$

Table 13: Measured values for the ξ_p $(= \ln(1/x_p))$ distribution.The first error is statistical, the second systematic.

n_{ch}	$P(n_{\mathrm{ch}})$				
6	0.033	$\pm$	0.040	$\pm$	0.078
8	0.39	$\pm$	0.23	$\pm$	0.20
10	1.51	$\pm$	0.56	$\pm$	0.45
12	2.86	$\pm$	0.53	$\pm$	0.31
14	5.54	$\pm$	0.78	$\pm$	0.42
16	8.8	$\pm$	1.0	$\pm$	0.5
18	11.2	$\pm$	1.1	$\pm$	0.4
20	11.3	$\pm$	1.0	$\pm$	0.8
22	10.8	$\pm$	1.0	$\pm$	0.7
24	10.1	$\pm$	1.0	$\pm$	0.6
26	8.9	$\pm$	0.9	$\pm$	0.8
28	6.96	$\pm$	0.76	$\pm$	0.36
30	5.29	$\pm$	0.65	$\pm$	0.21
32	4.25	$\pm$	0.60	$\pm$	0.54
34	3.46	$\pm$	0.52	$\pm$	0.41
36	2.49	$\pm$	0.49	$\pm$	0.27
38	1.84	$\pm$	0.41	$\pm$	0.31
40	1.55	$\pm$	0.42	$\pm$	0.45
42	1.13	$\pm$	0.45	$\pm$	0.70
44	0.55	$\pm$	0.24	$\pm$	0.29
46	0.30	$\pm$	0.17	$\pm$	0.22
48	0.56	$\pm$	0.38	$\pm$	0.39
50	0.09	$\pm$	0.12	$\pm$	0.10
52	0.00	$\pm$	0.12	$\pm$	0.05
54	0.10	$\pm$	0.11	$\pm$	0.08

Y	$1/\sigma \ \mathrm{d}\sigma_{\mathrm{ch}}/\mathrm{d}Y$
0.0 - 0.5	$7.18 \pm 0.28 \pm 0.23$
0.5 - 1.0	$7.44 \pm 0.26 \pm 0.15$
1.0 - 1.5	$7.64 \pm 0.25 \pm 0.13$
1.5 - 2.0	$6.53 \pm 0.22 \pm 0.26$
2.0 - 2.5	$6.00 \pm 0.21 \pm 0.31$
2.5 - 3.0	$5.22 \pm 0.20 \pm 0.15$
3.0 - 3.5	$3.71 \pm 0.17 \pm 0.15$
3.5 - 4.0	$2.33 \pm 0.13 \pm 0.17$
4.0 - 4.5	$0.90 \pm 0.08 \pm 0.07$
4.5 - 5.0	$0.47 \pm 0.06 \pm 0.05$
5.0 - 5.5	$0.06 \pm 0.02 \pm 0.02$
mean value	$1.758 \pm 0.014 \pm 0.003$

Table 14: Measured values of the probability of forming $\langle n_{\mathrm{ch}} \rangle$ charged particles (in %), and the Y distribution. The first error is statistical, the second systematic.

$p_\perp^{\rm in}$	$1/\sigma \;\; {\rm d}\sigma_{\rm ch}/{\rm d}p_\perp^{\rm in}$
0.0 - 0.1	$48.0 \pm 1.4 \pm 2.0$
0.1 - 0.2	$40.4 \pm 1.3 \pm 1.5$
0.2 - 0.3	$28.2 \pm 1.1 \pm 1.0$
0.3 - 0.4	$22.8 \pm 1.0 \pm 1.0$
0.4 - 0.5	$15.77 \pm 0.80 \pm 0.61$
0.5 - 0.6	$12.98 \pm 0.73 \pm 0.62$
0.6 - 0.7	$11.54 \pm 0.70 \pm 1.01$
0.7 - 0.8	$7.42 \pm 0.55 \pm 0.34$
0.8 - 0.9	$6.84 \pm 0.53 \pm 0.10$
0.9 - 1.0	$4.73 \pm 0.45 \pm 0.65$
1.0 - 1.2	$3.62 \pm 0.27 \pm 0.04$
1.2 - 1.4	$3.22 \pm 0.26 \pm 0.16$
1.4 - 1.6	$2.41 \pm 0.22 \pm 0.12$
1.6 - 2.0	$1.45 \pm 0.12 \pm 0.09$
2.0 - 2.5	$0.91 \pm 0.09 \pm 0.03$
2.5 - 3.0	$0.59 \pm 0.07 \pm 0.02$
3.0 - 3.5	$0.28 \pm 0.05 \pm 0.04$
3.5 - 4.0	$0.28 \pm 0.05 \pm 0.02$
4.0 - 5.0	$0.14 \pm 0.02 \pm 0.03$
5.0 - 6.0	$0.05 \pm 0.01 \pm 0.01$
mean value	$0.606 \pm 0.014 \pm 0.010$

$p_\perp^{\rm out}$	$1/\sigma \;\; {\rm d}\sigma_{\rm ch}/{\rm d}p_\perp^{\rm out}$
0.0 - 0.1	$71.4 \pm 1.7 \pm 2.1$
0.1 - 0.2	$55.5 \pm 1.5 \pm 1.4$
0.2 - 0.3	$37.4 \pm 1.2 \pm 1.5$
0.3 - 0.4	$25.3 \pm 1.0 \pm 1.1$
0.4 - 0.5	$16.10 \pm 0.80 \pm 0.28$
0.5 - 0.6	$9.85 \pm 0.62 \pm 0.47$
0.6 - 0.7	$6.17 \pm 0.49 \pm 0.19$
0.7 - 0.8	$4.44 \pm 0.42 \pm 0.49$
0.8 - 0.9	$2.78 \pm 0.33 \pm 0.34$
0.9 - 1.0	$1.82 \pm 0.26 \pm 0.19$
1.0 - 1.2	$1.27 \pm 0.16 \pm 0.15$
1.2 - 1.4	$0.59 \pm 0.11 \pm 0.08$
1.4 - 1.6	$0.29 \pm 0.07 \pm 0.03$
1.6 - 2.0	$0.20 \pm 0.04 \pm 0.02$
mean value	$0.261 \pm 0.004 \pm 0.010$

Table 15: Measured values for the $p_\perp^{\rm in}$ and $p_\perp^{\rm out}$ distributions. The first error is statistical, the second systematic.

	ξ_0	$\langle n_{\rm ch}\rangle$		D	$\langle n_{\rm ch}\rangle$/D	C_2	$\mathcal{R}_2$
		frag.	mult.				
standard result	3.94	23.40	23.61	7.63	3.10	1.104	1.062
stat. error	$\pm$0.05	$\pm$0.45	$\pm$0.45	$\pm$0.35	$\pm$0.13	$\pm$0.009	$\pm$0.009
event selection	$-$0.01	$-$0.39	$-$0.38	$-$0.26	$+$0.06	$-$0.004	$-$0.005
$\lvert\cos\theta_T\rvert < 0.7$	$-$0.05	$-$0.05	$-$0.14	$-$0.22	$+$0.07	$-$0.005	$-$0.005
track selection	$+$0.01	$-$0.16	$-$0.16	$-$0.18	$+$0.05	$-$0.004	$-$0.004
model dependence	$\pm$0.02	$\pm$0.25	$\pm$0.32	$\pm$0.23	$\pm$0.05	$\pm$0.003	$\pm$0.004
fit function	$-$0.08	–	–	–	–	–	–
fit range	$\pm$0.05	–	–	–	–	–	–
unfolding	–	–	$-$0.12	$-$0.11	$+$0.03	$-$0.002	$-$0.002
tot. syst. error	$\pm$0.11	$\pm$0.47	$\pm$0.55	$\pm$0.46	$\pm$0.12	$\pm$0.008	$\pm$0.009

Table 16: Results with statistical and systematic uncertainties for the position ξ_0 of the peak in the ξ_p distribution, for $\langle n_{\rm ch}\rangle$ based on the fragmentation function (frag.) or the multiplicity distribution (mult.), and for the dispersion D, the ratio $\langle n_{\rm ch}\rangle$/D and the second moments C_2 and $\mathcal{R}_2$. The signs indicate the direction of the changes.

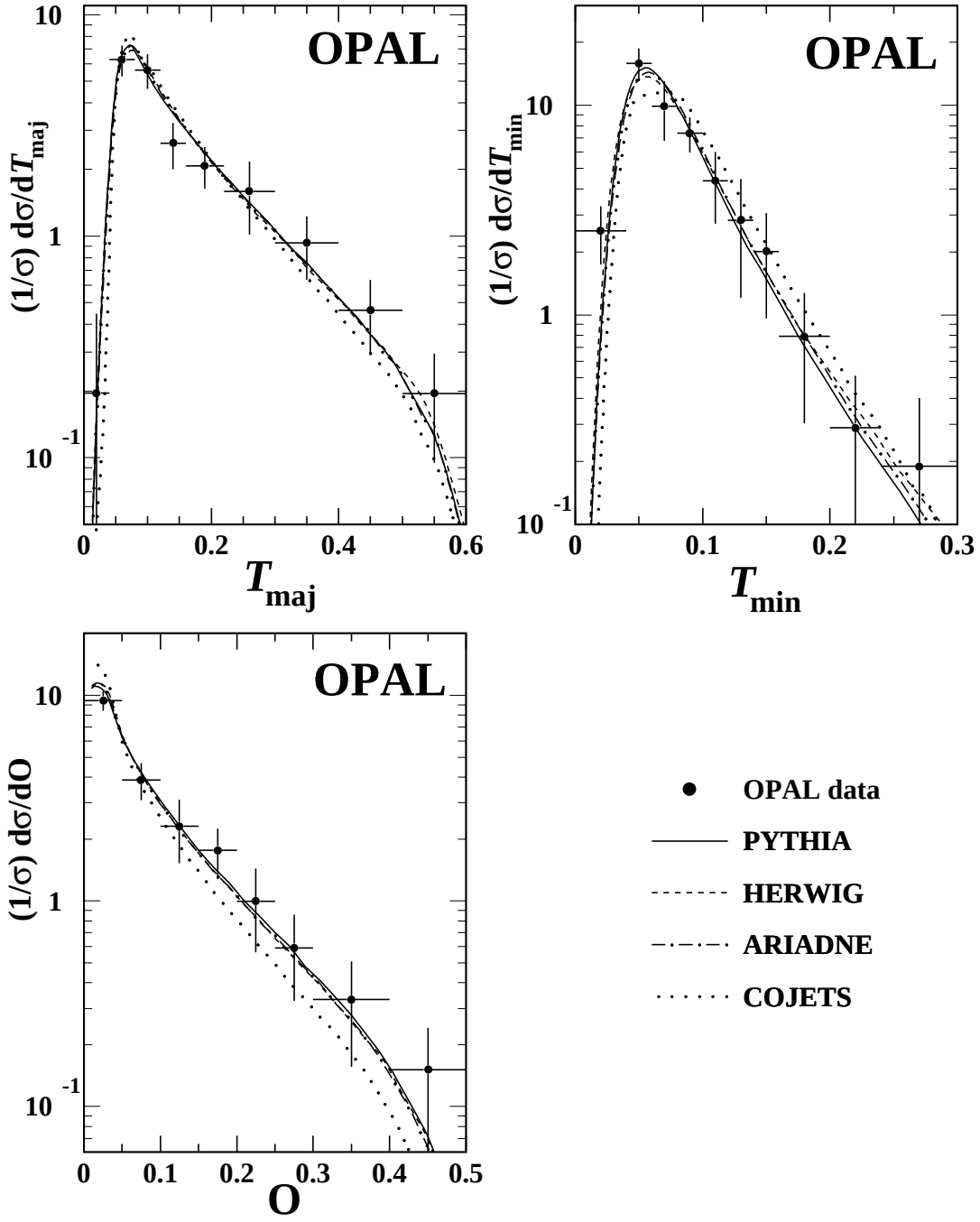

Figure 1: Distributions of $T_{\rm maj}$, $T_{\rm min}$, and Oblateness. Statistical and systematic errors are shown added in quadrature.

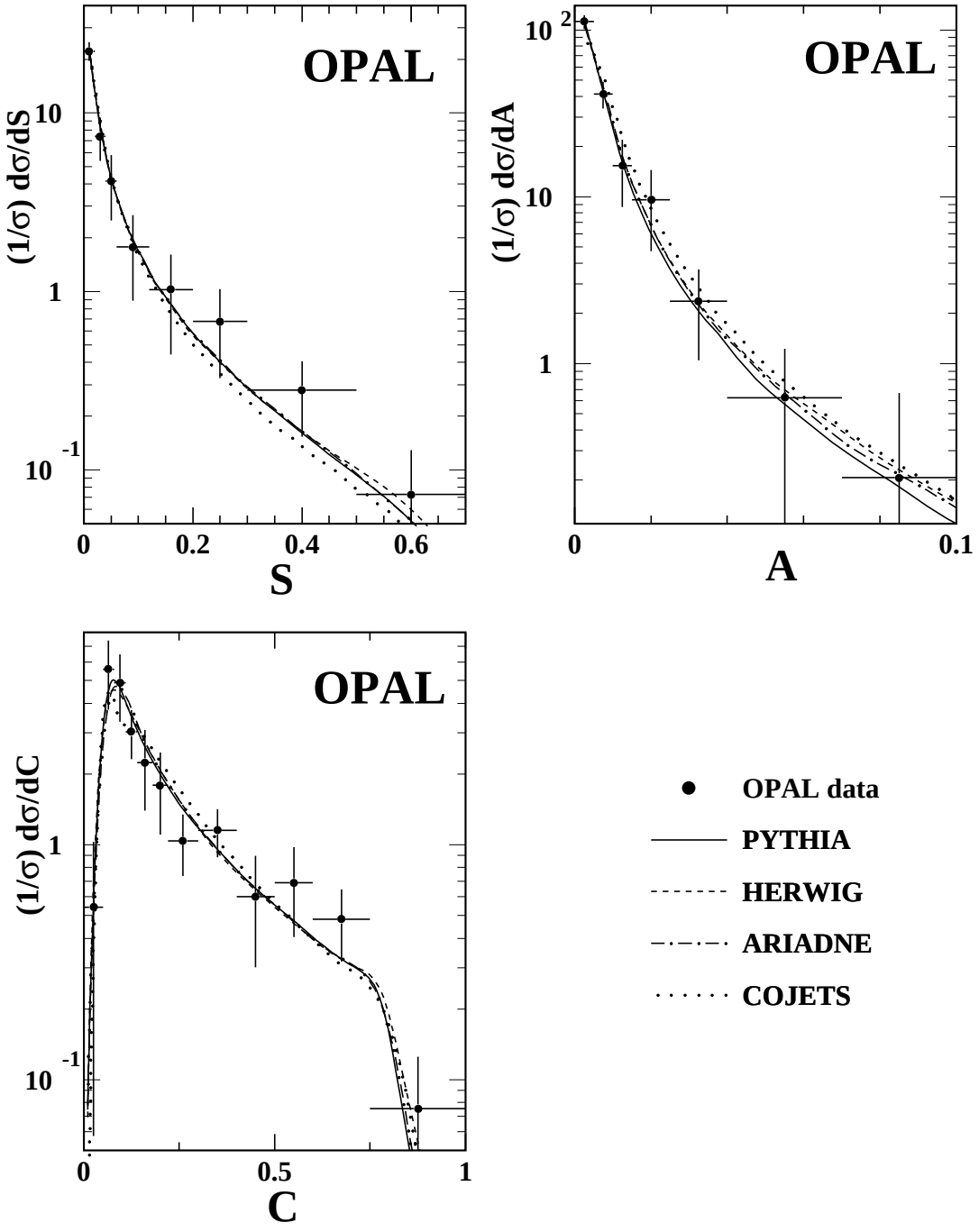

Figure 2: Distributions of Sphericity, Aplanarity and C-parameter. Statistical and systematic errors are shown added in quadrature.

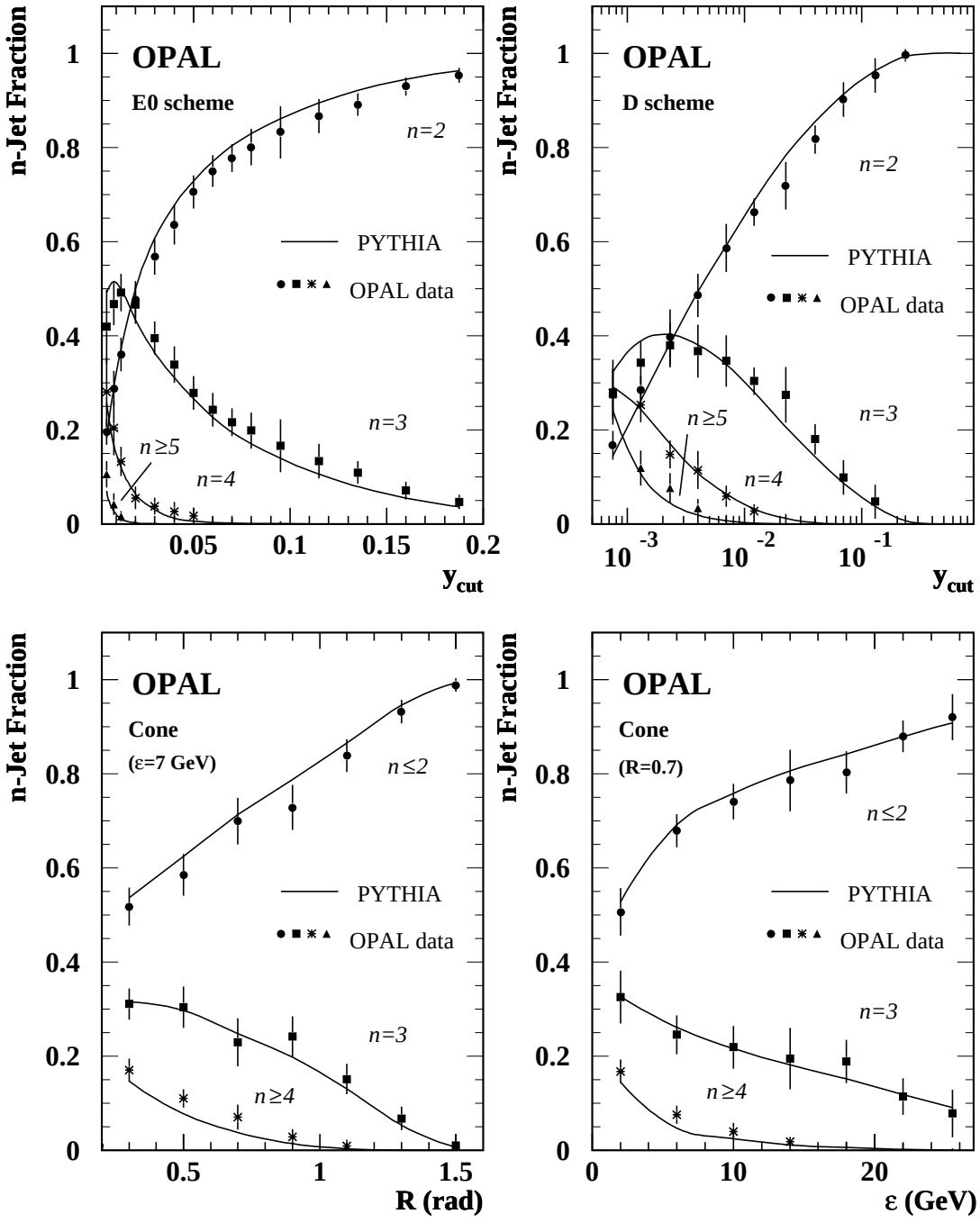

Figure 3: The figure shows fractions of 2-, 3-, 4-, and 5-and-more jet events as functions of the jet resolution parameters $y_{\rm cut}$ for the E0 and the D jet finding scheme, and as functions of energy cutoff ε or cone half angle R for the cone jet finder. The prediction of the PYTHIA Monte Carlo is shown by the lines.

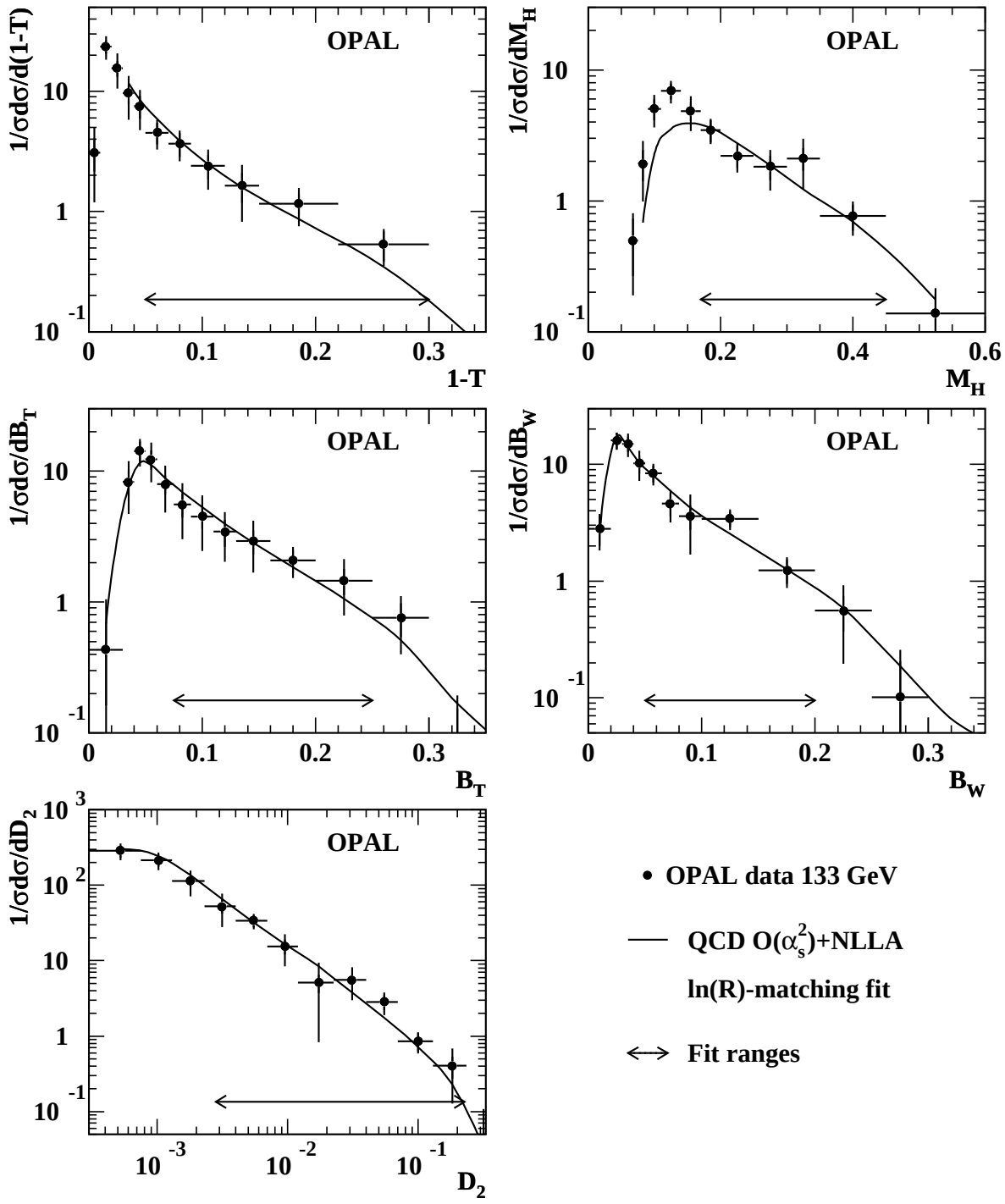

Figure 4: Fits of $\mathcal{O}(\alpha_s^2)$+NLLA QCD predictions to event shape observables. The data points are corrected to hadron level, and the errors shown are statistical and systematic added in quadrature. The fitted regions are indicated by arrows.

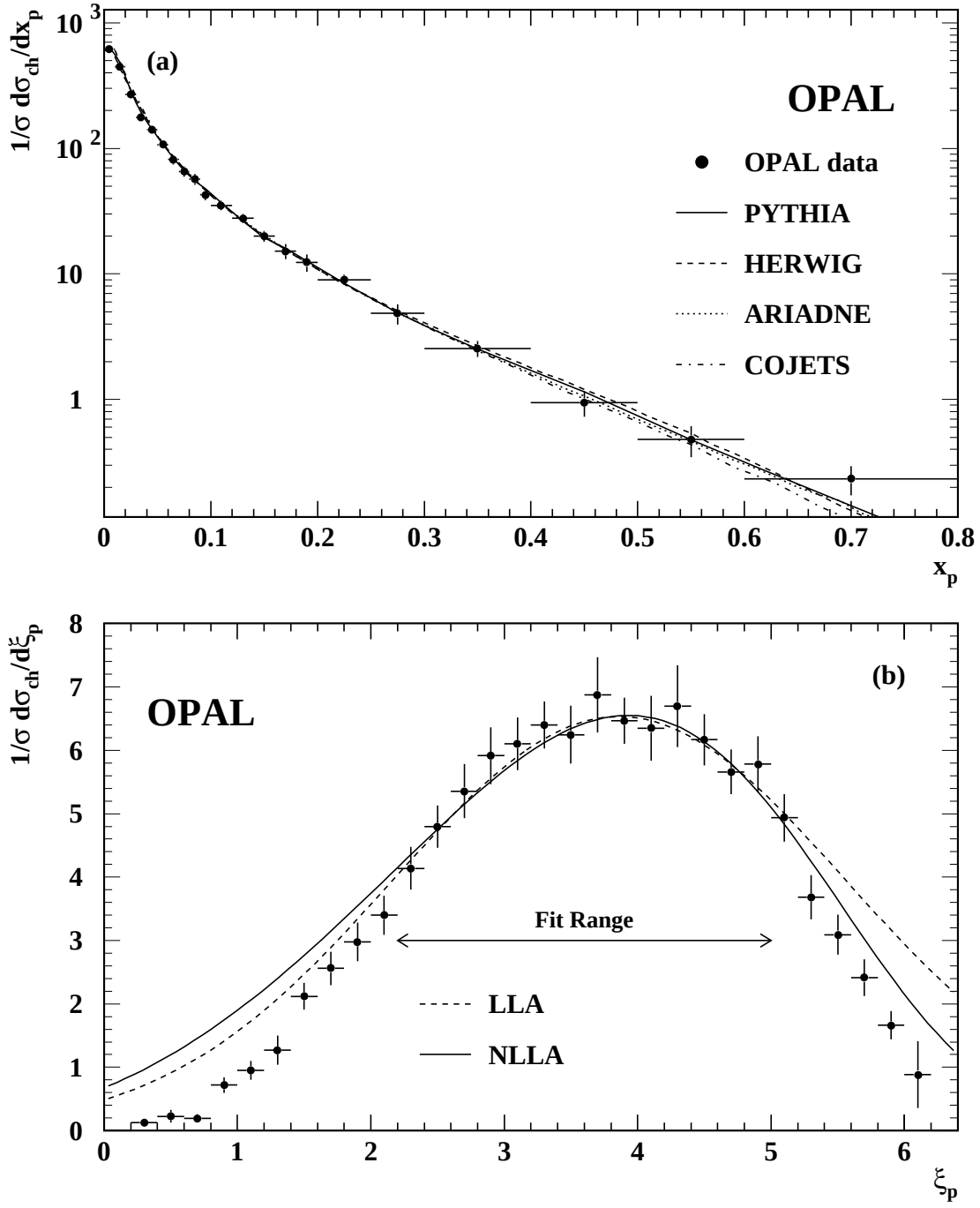

Figure 5: (a) Distribution of x_p compared to the predictions of Monte Carlo models. (b) Distribution of ξ_p fitted by NLLA (solid) and LLA (dashed) predictions. The fits are performed in the range indicated and extrapolated to other ξ_p values.

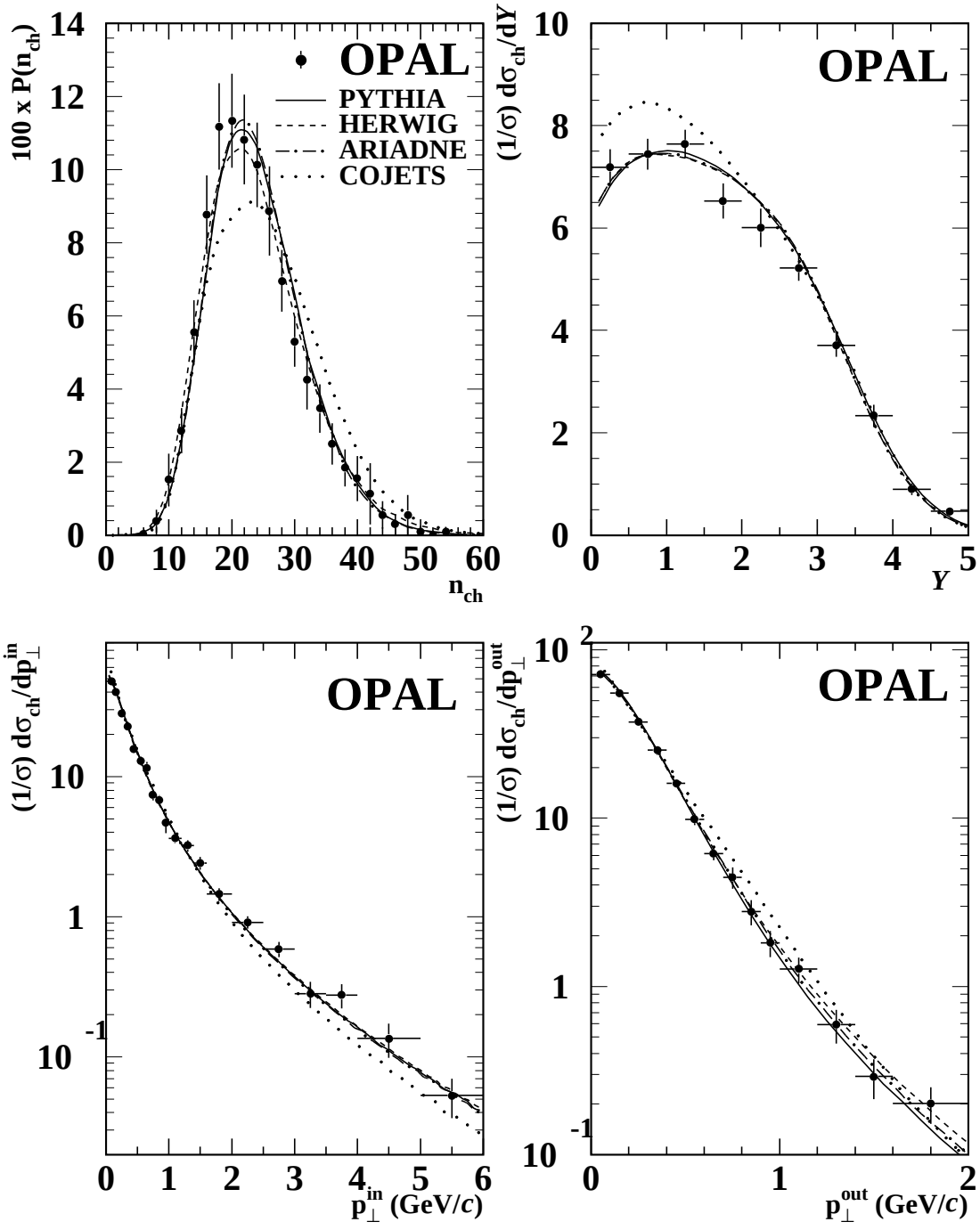

Figure 6: Distributions of multiplicity $P(n_{\rm ch})$, rapidity Y, $p_\perp^{\rm in}$ and $p_\perp^{\rm out}$ with statistical and systematic errors shown added in quadrature.

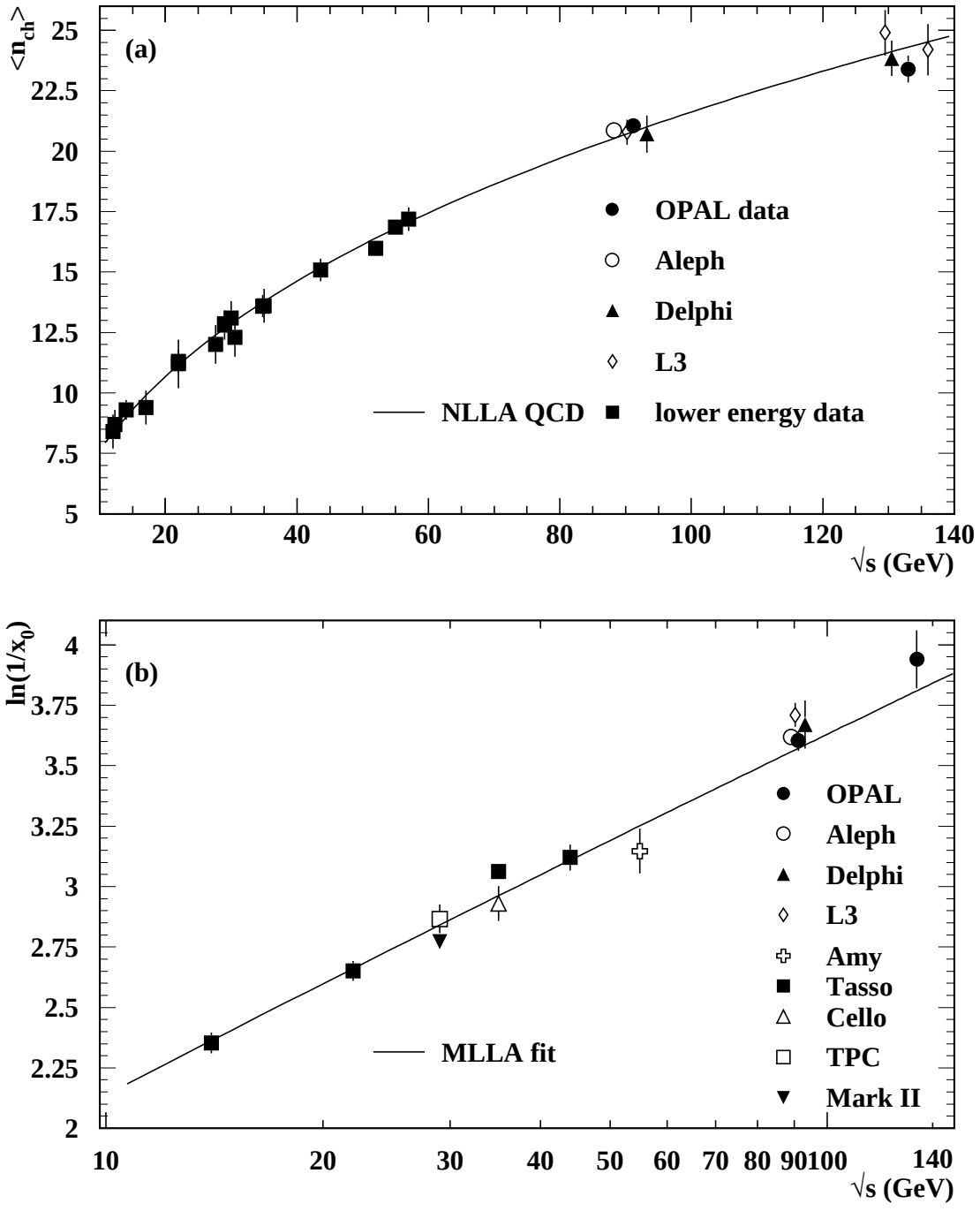

Figure 7: (a) Charged multiplicity values measured at several energies plotted together with a fit of a NLLA QCD prediction. (b) Values of the position of the peak ξ_0 ($= \ln(1/x_0)$) of the ξ_p distribution measured at several energies plotted together with a fit of a MLLA QCD prediction.

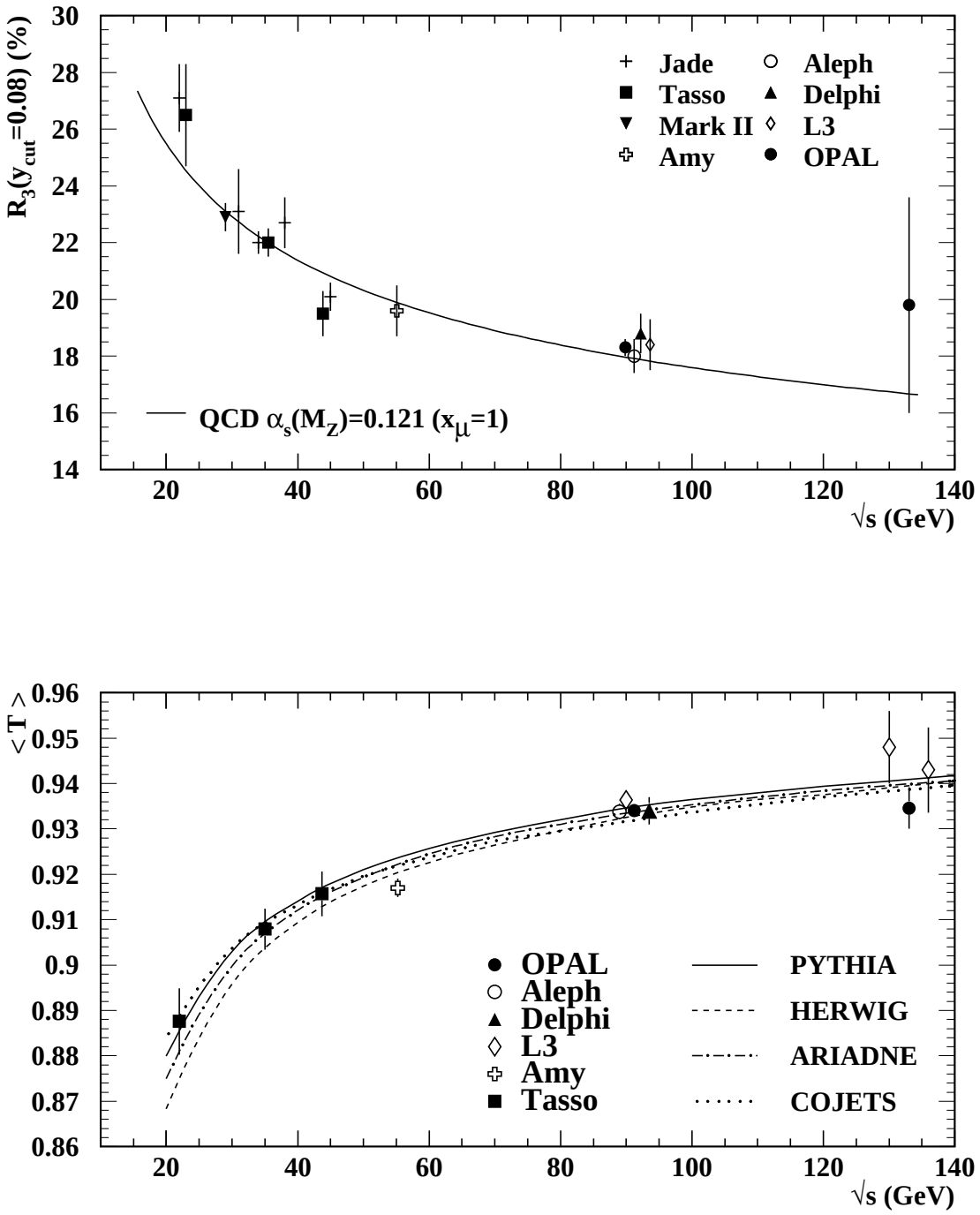

Figure 8: Distributions of (a) R_3 at $y_{\rm cut}$=0.08 for the JADE E0 algorithm and (b) mean value of thrust $\langle T \rangle$ at several energies.

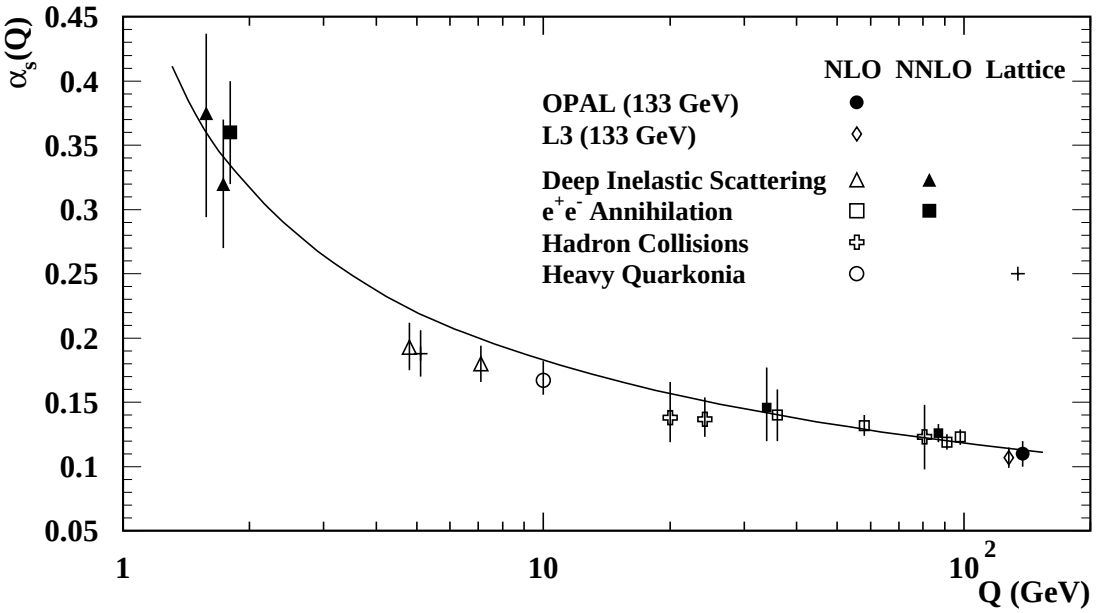

Figure 9: Values of α_s at different energies. The labels NLO and NNLO refer to the order of calculations fitted to extract α_s measurements. NLO corresponds to $\mathcal{O}(\alpha_s^2)$ in e^+e^- annihilations, and NNLO to $\mathcal{O}(\alpha_s^3)$. The label Lattice refers to α_s values determined from lattice QCD calculations. The curve shows the second order QCD prediction for α_s with $\alpha_s(M_{Z^0})$=0.120.